Andean Geology 45 (1): 47-77. January, 2018
doi: 10.5027/andgeoV45n1-3036

Andean Geology
www.andeangeology.cl

Tephra fallout from the long-lasting Tungurahua eruptive cycle (1999-2014): Variations through eruptive style transition and deposition processes

***Jorge Bustillos A.[1], Jorge E. Romero[2], Alicia Guevara C.[3], Juan Díaz-Alvarado[2]**

[1] *Facultad de Geología Minas, Petróleos y Ambiental, Carrera de Ingeniería en Geología, Universidad Central del Ecuador, casilla 872 A, Quito, Ecuador.*
jebustillos@uce.edu.ec

[2] *Departamento de Geología, Universidad de Atacama, Avda. Copayapu 485, Copiapó, Chile.*
jorge.romerom@alumnos.uda.cl; juan.diaza@uda.cl

[3] *Departamento de Metalurgia Extractiva, Escuela Politécnica Nacional, Avda. Ladrón de Guevara E11-253 Quito, Ecuador.*
alicia.guevara@epn.edu.ec

***** *Corresponding author: jebustillos@uce.edu.ec*

ABSTRACT. The Tungurahua volcano (Northern Andean Volcanic Zone) has been erupting since 1999, with at least four eruptive phases up to present. Although a dozen of research focuses in tephra fall deposits during this period, none of them cover the full eruptive cycle. We investigated the eruptive mechanisms and tephra fall deposition processes at Tungurahua between 1999 and 2014, through systematic analyses of tephra samples collected westward of the volcano using mechanical sieving grain size analysis, lithology, scanning electron microscopy, X-Ray fluorescence and X-Ray diffraction. Tephra is compounded by varying amounts of scoria (black and brown), lithics, hydrothermally altered fragments, pumice, glass shards and free crystals. Textural analyses of juvenile grains (scoria, pumice and glass shards) revealed a diversity of features concerning to their vesicularity, shape and surface/perimeter. Initially, tephra was characterized by hydrothermally altered fragments related to a phreatic phase which then evolved to a pure magmatic activity with Strombolian eruptions. A homogeneous andesitic composition was observed between 1999 and 2003; however silica-rich compositions occurred later in 2006. Similarly, the mineral assemblage contained plagioclase, pyroxene and olivine, but magnetite and akermanite were then included during 2006, thus indicating the eruption of a new, probably mixed magma. As consequence, Plinian activity occurred in August 2006. Further activity in 2007 ejected notable amounts (40-65%) of recycled material during Vulcanian eruptions. New eruptions occurred between 2008 and 2010, and juvenile ash revealed the interplay between brittle and ductile fragmentation through ash explosions, jetting events and Strombolian activity. The activity between 2010 and 2012 incorporated hydrothermally altered material at time that eruptive silences became longer and frequent, thus suggesting the development of a sporadic hydrothermal system. Finally, between 2013 and 2014 a series of Vulcanian events occurred. Observed grain size distributions allow us to propose three different processes occurring during tephra deposition: **1)** deposition of multiple ash plumes, **2)** contributions from elutriated pyroclastic density currents or grain size mixing due to major eruptions, and **3)** the aggregation of particles due to rain and/or lighting. From mineralogy and grain size we infer that exposition to ash may produce acute human health effects.

Keywords: Eruptive mechanism, Tephra fall deposits, Andesitic volcanism, Tungurahua volcano.

RESUMEN. Caída de tefra del ciclo eruptivo de larga duración del volcán Tungurahua (1999-2014): variaciones a través de las transiciones de estilo eruptivo y de los procesos depositacionales. El volcán Tungurahua (Zona Volcánica Norte de los Andes) inició, el año 1999, un proceso eruptivo y desde entonces han acontecido al menos cuatro fases eruptivas. Aunque una docena de investigaciones se centran en los depósitos de tefra acumulados durante este período, ninguno de ellos cubre el ciclo eruptivo completo. Se investigaron los mecanismos eruptivos y los procesos de depositación de la tefra entre 1999 y 2014, a través de análisis sistemáticos de muestras de tefra recolectadas al oeste del volcán, utilizando análisis mecánico de granulometría, litología, microscopía electrónica de barrido, fluorescencia de rayos X y difracción de rayos X. La tefra está compuesta por cantidades variables de escoria (negra y marrón), líticos, fragmentos alterados hidrotermalmente y fragmentos de pómez, vidrio y cristales. Los análisis texturales de fragmentos juveniles (escoria, pómez y vidrio) revelaron diversas características en cuanto a su vesicularidad, forma y superficie/perímetro.

En la etapa inicial del proceso eruptivo, la tefra se caracterizó por la presencia de fragmentos alterados hidrotermalmente relacionados con una fase freática, que luego evolucionó a una actividad magmática con erupciones estrombolianas. La composición química y mineralógica del material juvenil de las tefras indica una composición andesítica homogénea para el magma eyectado entre los años 1999 y 2003; sin embargo, composiciones ricas en sílice se produjeron posteriormente en 2006. De forma similar, el conjunto mineral contenía plagioclasa, piroxeno y olivino, pero se incluyeron magnetita y akermanita durante 2006, indicando un cambio en la composición del magma, probablemente mezclado. Como consecuencia de este cambio, en agosto 2006 ocurrió una erupción pliniana. La actividad eruptiva en el año 2007 arrojó cantidades notables (40-65%) de material reciclado durante erupciones vulcanianas. Nuevas erupciones ocurridas entre los años 2008 y 2010, y el material juvenil de la ceniza eyectada reveló la interacción entre fragmentación frágil y dúctil a través de explosiones de cenizas, eventos de chorro y actividad estromboliana. La actividad entre los años 2010 y 2012 incorporó material hidrotermalmente alterado durante silencios eruptivos, los que se hicieron más frecuentes y prolongados, sugiriendo así el desarrollo de un sistema hidrotermal esporádico. Finalmente, entre 2013 y 2014 ocurrieron una serie de erupciones Vulcanianas. La distribución de tamaño del grano observada en los depósitos de tefra nos permite proponer tres procesos diferentes que ocurren durante su depositación: **1)** depositación múltiple de plumas de ceniza, **2)** contribuciones de corrientes de densidad piroclásticas elutriadas o mezclas de granulometría debido a grandes erupciones, y **3)** agregación de partículas debido a la lluvia y/o tormentas eléctricas. A partir de la mineralogía y tamaño de grano inferimos que la exposición a la ceniza puede producir efectos agudos en la salud humana.

Palabras clave: Mecanismo eruptivo, Depósitos de caída de tefra, Volcanismo andesítico, Volcán Tungurahua.

1. Introduction

Studies of geochemical, mineralogical and lithological properties of tephra fall deposits are currently used as robust analytical tools for the complementary description of eruptive styles and processes (Cioni *et al.,* 2008; Tsunematsu and Bonadonna, 2015). As inherited characteristics from these eruptive processes, the shape and nature of the main constituents of volcanic ash reflect explosive mechanisms of volcanic eruptions, and their transition in time contribute to forecast the changes of ongoing eruptive events (Dellino and Volpe, 1995; Cannata *et al.,* 2014; Clarke *et al.,* 2015; Taddeucci *et al.,* 2015). Besides, determination of tephra grain size distribution (GSD) provide important insights into fragmentation mechanisms, eruptive conditions, tephra deposition and volcanic hazards at active volcanoes (*e.g.,* Walker, 1971; Carey and Sigurdsson, 1982; Bonadonna *et al.,* 2002; Houghton and Carey, 2015). In fact, understanding the eruption mechanisms is critical for improving hazard assessment during volcanic crises. This is especially important at long-lasting eruptions for the recognition and mitigation of evolving volcanic hazards through time.

Tungurahua volcano (01º28' S; 78º27' W, 5,019 m a.s.l., Fig. 1) is an active andesitic strato-volcano at the Northern Andean Volcanic Zone (NAVZ; Kley *et al.,* 1999), distant 120 km south of Quito (Ecuador), with a record of five post-Columbian eruptive cycles (1641, 1773, 1886, 1916-18 and 1999 to the time of writing). Since 1999 and up to 2014, Tungurahua volcano has erupted *ca.* 0.13 km^3 of bulk tephra, frequently dispersed towards its west flank, through various types of volcanic activity in four major eruptive phases (Bustillos *et al.*, 2016). Several studies with different techniques have included the analysis of these tephras in very specific time periods such as those of 1999-2001, 2006, 2010, 2012, 2013, and 2014 (*e.g.*, Le Pennec *et al.*, 2004; Ruiz *et al.*, 2004; Troncoso *et al.*, 2006; Bustillos, 2010; Bustillos *et al*., 2011; Le Pennec *et al*., 2012; Eychenne *et al*., 2012; Bustillos *et al.,* 2013; Bernard *et al.*, 2013; Eychenne *et al*., 2013; Parra *et al.*, 2015; Romero *et al.*, 2017). Currently, there is not a continuous database of tephras between 1999 and 2013 in Tungurahua, doing harder to establish their variations through eruptive-style transitions and their related feeding mechanisms. In the current contribution, we study the temporal variations of tephra fallouts as consequence of changing eruption mechanisms between 1999-2014 at Tungurahua volcano. We also look at the amount of fine ash ejected by the volcano for health hazard considerations. Overall, our work provides a comprehensive dataset on the characteristics of ash erupted by Tungurahua during fifteen years of eruptive activity.

2. Geological and Volcanological Settings

2.1. Geological background

The volcanoes of the Northern Andean Volcanic Zone are mainly andesitic and dacitic, although

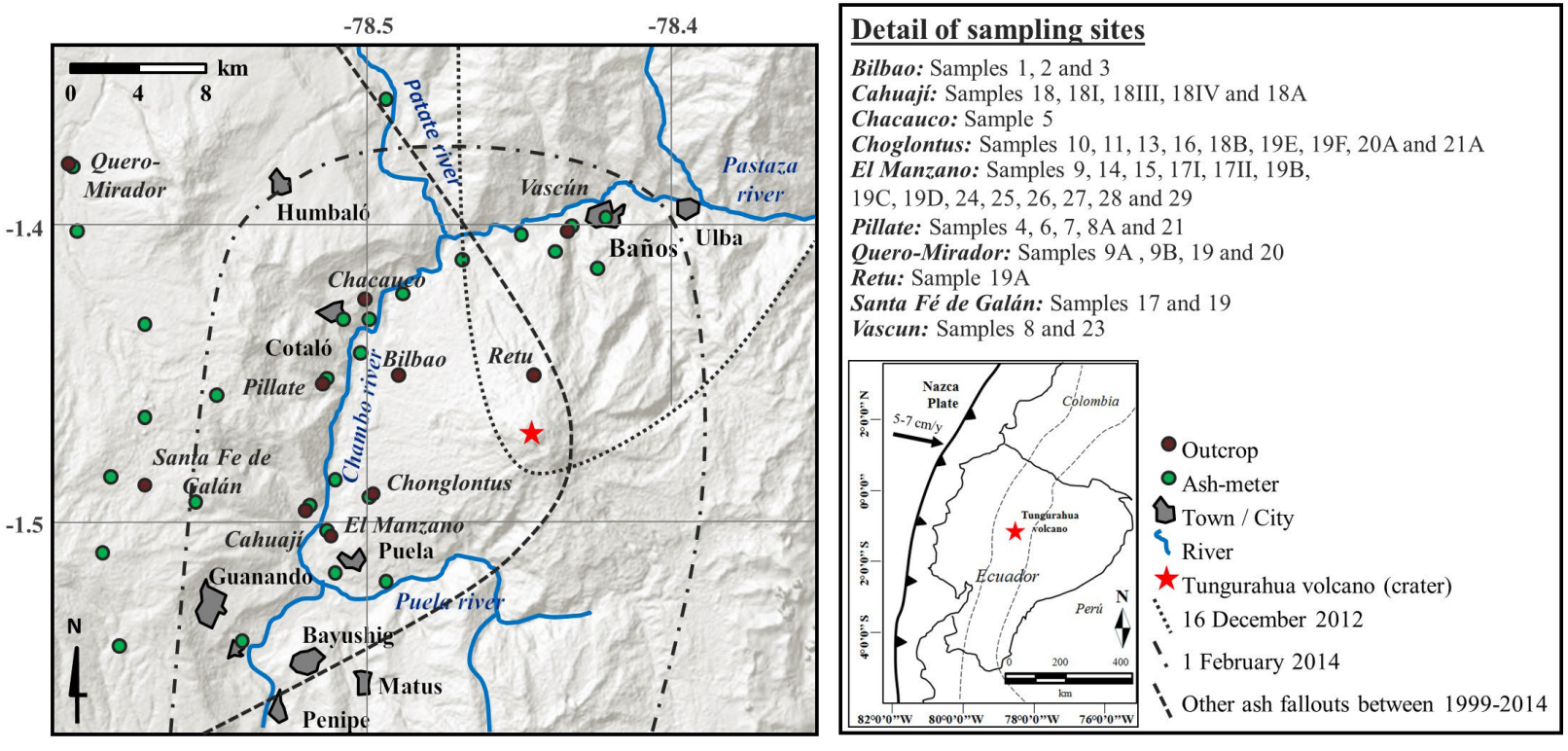

FIG. 1. Location of Tungurahua volcano. The sampling sites in outcrop (brown dots) and the location of ash-meters (green dots) administered by IG-EPN are included in the map. See legend for details on the sampling sites and their correspondent samples. Dispersion of relevant tephra falls are indicated as dashed lines.

basaltic andesites and rhyolites also occur (Stern, 2004). The Ecuadorian active continental volcanism is distributed in two main chains: Western Cordillera and Eastern Cordillera, but also along the Inter-Andean valley and in the back-arc position (Hall *et al.,* 2008). The youngest eruptive products at the Eastern Cordillera are low-to high-silica andesites with a typical calc-alkaline affinity (56-61 wt% SiO_2; Hall *et al.,* 2008). Tungurahua volcano is located at Eastern Cordillera, and it corresponds to an andesitic to dacitic stratovolcano (54-67 wt% SiO_2; Hall *et al.,* 1999), whose edifice elevates 3 km height above its basement made of Paleozoic to Cretaceous age rocks, locally intruded by granitic plutons of Paleozoic to Jurassic ages (Litherland and Egüez, 1993; Aspden *et al.,* 1994; Le Pennec *et al.,* 2008; Le Pennec *et al.,* 2012). The volcano consists of three edifices (Tungurahua I, II, and III), while two sector collapses are recognized to have occurred 30 ky and 3 ky BP (Hall *et al.,* 1999; Molina *et al.,* 2005; Le Pennec *et al.,* 2006; Bustillos*,* 2008). The youngest edifice (Tungurahua III) grew inside the last collapse scarp (3 ky BP), on the western flank of the Tungurahua II stratocone (Le Pennec *et al.,* 2008). Since ~700 ^{14}C yr BP the activity has included pyroclastic density currents (PDCs) and tephra falls, with a period of notable eruptive activity during the 14th century (Le Pennec *et al.,* 2008).

2.2. Eruptive activity since 1999

Historical eruptions took place in 1641-1646, 1773-1781, 1886-1888, 1916-1918, leading up to the current eruptive cycle which began in 1999 and persists until the time of writing (Almeida and Ramón, 1991; Hall *et al.,* 1999; Le Pennec *et al.,* 2008). According to Bustillos *et al.* (2016), Tungurahua volcano has erupted a cumulative tephra volume of 130 Mm^3 between 1999 and 2014 (about 42 Mm^3 were erupted only in 2006 eruptions; Eychenne *et al.*, 2012), which in most of cases (~70%) has affected its western flank due to the prevailing wind direction in that area (Fig. 1; Le Pennec *et al.*, 2012; Bernard *et al.*, 2013; Parra *et al.*, 2015). In addition, the average non-DRE (Dense Rock Equivalent) tephra deposition rate increased from ~8,700 m^3/day to ~19,000 m^3/day after the 2006 explosive phases (Bustillos *et al.,* 2016). Maps showing actual distributions of fallout and PDC deposits from representative eruptions are available from Eyechenne *et al.* (2012); Le Pennec *et al.* (2012); Eychenne *et al.* (2013), Bernard *et al.* (2013), Bernard *et al.* (2016) and Bustillos *et al*. 2016. The current eruptive cycle has experienced four phases between 1999 and 2013 (Bustillos *et al.*, 2016) (Fig. 2).

2.2.1. Phase I (1999-2005)

The reawakening of Tungurahua was progressive between August and October 1999, with a phreatic vent-clearing onset followed by magmatic activity in mid-October, and then by alternating phases of gas and ash emissions, Strombolian to violent Strombolian eruptions and many canon-like shots associated with short-lived "Vulcanian-like" explosions (Ruiz *et al.,* 2006; Le Pennec *et al.,* 2012). After seven months of quiescence, deep LP seismicity announced a new eruption beginning in late May 2001, which developed small-scale lava fountains and explosions in June and July (Le Pennec *et al.,* 2002). Prior to the August 4th 2001 eruption, precursory activity was not recorded and surface phenomena consisted of Strombolian to violent Strombolian activity, including a lava fountaining event by August 16th before the waning of eruption in August 21st (Le Pennec *et al.,* 2012). New activity dominated by Strombolian phases produced sub-regional to regional ash falls that persisted until 2005 (Mothes *et al.,* 2015). Samaniego *et al.* (2011) proposed that episodic injections fed magma to a modest reservoir 10 km bellow Tungurahua's crater, which in turn supplied magma to the surface between 1999 and 2005. However, Wright *et al.* (2012) concluded that variable magma supply rates better explain the transition between Vulcanian and Strombolian styles through an almost persistent eruptive activity.

2.2.2. Phase II (July-August 2006)

Precursory signals as deep long-lasting seismic activity (5-15 km below the summit) in early April 2006 and edifice deformation consistent with the intrusion of 4.5 Mm^3 of magma were registered between March 10th and April 14th 2006 (Champenois *et al.,* 2014). The intrusion of a new, hot and volatile-rich magma batch probably disrupted the more evolved and degassed magma reservoir of Tungurahua, leading to the dramatic Plinian eruptions of 2006 (*e.g.,* Samaniego *et al.,* 2011; Eychenne *et al.,* 2013; Myers *et al.,* 2014). The first eruption took place on July 14th, with a 10 km-high (above the crater) tephra column and several scoria flows that descended by

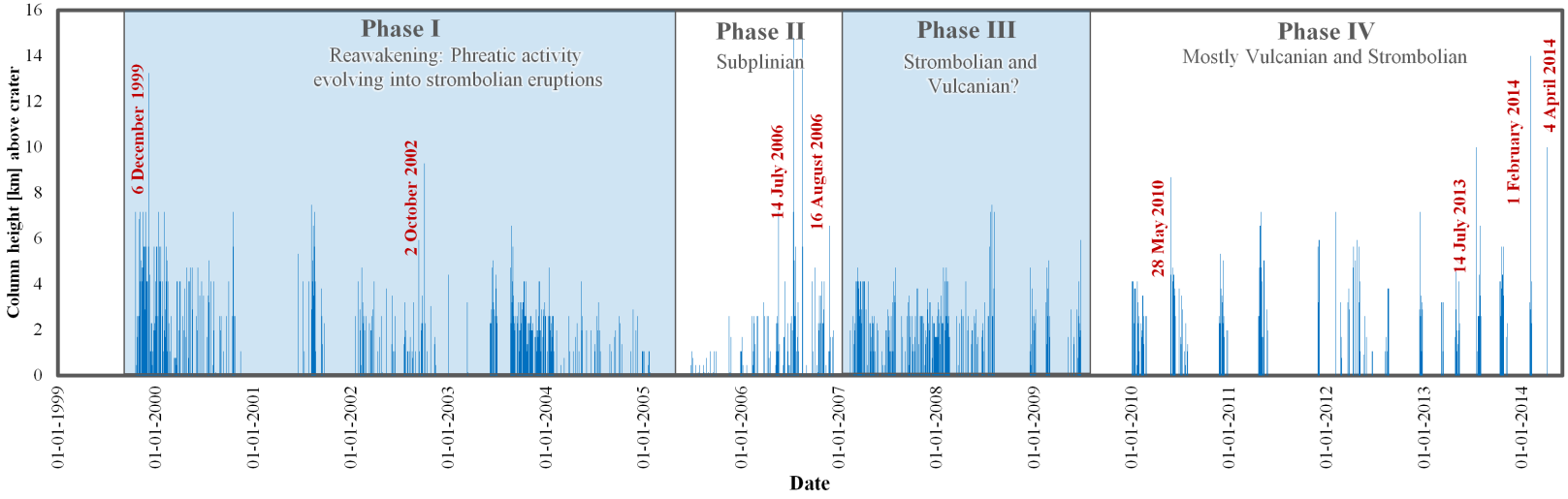

FIG. 2. Eruptive phases during the 1999-2014 eruptive cycle at Tungurahua volcano as defined by Bustillos *et al.* (2016) combining direct observation, available data published for each eruption (see references therein), and column heights (km above the crater).

the western flank of the cone. The second eruption occurred after a rapid increase of seismic activity in the morning of August 16th, and consisted of a sustained eruption that started at 22:00 h UTC leading to a paroxysmal phase about 05:15 h UTC on August 17th and lasted around 50-60 min. (Eyechenne *et al.,* 2013). The July 14th eruption ejected about 1.0 Mm^3 of dense rock equivalent (DRE) products, while the August 16-17th eruptions produced a stratospheric column (~14 km above the crater) with the ejection of *ca.* 7.7 Mm^3 of DRE juvenile tephra and a 18.7 Mm^3 of DRE PDCs (Steffke *et al.,* 2010; Eyechenne *et al.,* 2012*,* 2013; Hall *et al.,* 2013; Douillet *et al.,* 2013a, 2013b). Eychenne *et al.* (2013) estimated both the July 14th and August 16-17th eruptions to be of volcanic explosivity index (VEI) values of 2 and 3, from ground based data.

2.2.3. Phase III (2007-2009)

Beginning in August 2007, heightened seismic activity associated with explosion events and jetting activity was recorded up to the February 2008 eruption, and even a ground uplift (17.5 cm in vertical axis) originated in the upper western flank was visible in interferograms that span the period December 26th 2007 to March 27th 2008, probably triggered by a magma intrusion of 1.2 Mm^3 (Biggs *et al.,* 2010). Following the February 2008 Vulcanian eruption, the volcano experienced a period of relative quiescence with a few small explosions and jetting tremors recorded (Biggs *et al.,* 2010). Since 2008, short- to medium-lived Strombolian eruptions have occurred, spanning from a few days to a few weeks, separated by periods of quiescence ranging from two to six months (Bernard *et al.,* 2013).

2.2.4. Phase IV (2010 to the present)

Since 2010, the activity has been interspersed by Vulcanian eruptions with varying intensity, often accompanied by explosions as well as small PDCs, some of them reaching the volcano's base (Mothes *et al.,* 2015; Hall *et al.,* 2015; Parra *et al.,* 2015; Romero *et al.*, 2017). One of the largest Vulcanian events recorded at Tungurahua during the current eruptive cycle occurred in February 1st 2014, with a minimum erupted volume of about 1.2 Mm^3 of PDCs and 4.5-6.4 Mm^3 of air fall tephra (Hall *et al.,* 2015; Romero *et al.*, 2017). These Vulcanian events are preceded by abrupt onsets or little precursory activity (*e.g.,* Kim *et al.,* 2014; Hall *et al.,* 2015; Parra *et al.,* 2015; Romero *et al.*, 2017).This is in agreement with volcano degassing, which was more or less continuous between 1999 and late 2008, but then changed to episodic activity without significant degassing during quiescence periods (Arellano *et al.,* 2008; Hidalgo *et al.,* 2015).

3. Sampling and analytical methods

3.1. Tephra samples

For this study we analyzed 47 samples collected between 1999 and 2013 (Fig. 1; Table 1). The ash samples from 1999 to 2005 were systematically collected by members of the Instituto Geofísico of Escuela Politécnica Nacional (IG-EPN) at distances of 5-20 km from the crater. The samples have been preserved in cool and dry conditions. During the catastrophic 2006 explosive activity, tephra sampling was carried out as soon as possible after the eruptive activity (<24 h). Since 2007 and up to 2012, the IG-EPN members used a series of "ash-meters" which consist of plastic recipients 20 cm diameter and 20 cm height, installed at a distance <20 km from the crater (Bustillos, 2010; Bustillos and Mothes, 2010). These ash-meters were installed below the most frequent dispersal pattern of the ash, to the west of the volcano (Fig. 1). This instrumental monitoring, the reports of volcanic activity, and sample collection have been also enhanced by the help of volunteer community members since 2000, locally known as *vigías* (watchmen) (*e.g.,* Stone *et al.,* 2014; Mothes *et al.,* 2015).

3.2. Tephra lithologies and textures

The lithological and textural descriptions of tephra components are based on the standard classification of Heiken and Wholetz (1985). We used two main procedures for the lithology and texture characterization of ash samples: **1)** Representative tephra samples (homogenized, quartered and <2 mm diameter; coarse to very fine ash) were analyzed using a binocular microscope. The relative proportions (%) of each particle type were determined through hand picking using fine forceps. They were distributed over glass plates, allowing the identification of their components. **2)** By using the scanning electron microscope (SEM), a technique used since the last decades for description of ash particles

TABLE 1. PHYSICAL FEATURES OF THE SAMPLES ANALYZED WITHIN THIS CONTRIBUTION.

Sample	D (km)	Date	Mass (g)	Bulk density (g/cm3)	True density (g/cm3)	Porosity (%)
1	7.4	06.10.1999	28.86	1.625	2.699	39.8
2	7.4	21.07.2000	94.6	1.782	2.79	36.1
3	7.4	10.08.2001	16.28	1.705	2.748	38
4	8.5	16.09.2001	47.36	1.421	2.727	47.9
5	8.5	17.03.2002	30.61	1.334	2.612	48.9
6	8.3	02.10.2002	60.58	1.42	2.771	48.8
7	8.3	07.10.2003	11.08	1.336	2.618	49
8	8.4	08.11.2003	106.61	1.569	2.689	41.7
8A	8.4	17.07.2004	-	-	-	-
9	6.5	20.04.2006	69.71	1.45	2.779	47.8
9A	21	26.05.2006	301.86	1.54	2.705	43.1
9B	21	24.08.2006	458.56	1.233	2.753	55.2
10	6.6	27.07.2007	321.523	1.58	2.765	42.9
11	6.6	05.08.2007	78.32	1.588	2.878	44.8
12	13	09.12.2007	117.64	1.393	2.648	47.4
13	6.6	05.02.2008	32.36	0.614	2.341	73.8
14	6.5	06.02.2008	79.9	0.666	2.588	74.3
15	6.6	07.02.2008	78.82	1.375	2.709	49.2
16	13	10.02.2008	102.57	1.493	2.695	44.6
17	9.5	21.06.2009	12.11	1.445	2.733	47.1
I	9.5	01.01.2010	-	1.017	2.527	59.8
II	9.5	10.02.2010	-	1.353	2.72	50.3
18	6.6	17.02.2010	191.31	1.38	2.775	50.3
18 I	3.2	28.05.2010	30.06	-	-	-
III	21	28.05.2010	-	0.665	2.028	67.2
IV	21	22.11.2010	-	1.51	2.868	47.4
18A	8.3	23.12.2011	39.45	1.433	2.775	48.4
18B	6.6	27.12.2011	71.76	1.543	2.694	42.7
19 A	3	04.02.2012	58.07	1.191	2.52	52.7
19	21	10.02.2012	383.63	1.358	2.626	48.3
19B	6.5	23.02.2012	131.65	-	-	-
19C	6.5	17.06.2012	293.67	-	-	-
19D	6.5	23.06.2012	103.53	-	-	-
19E	6.6	10.08.2012	29.98	-	-	-
19F	6.6	13.08.2012	36.63	-	-	-
20	21	23.08.2012	248.37	1.223	2.709	54.9
20A	6.6	23.08.2012	40.07	-	-	-
21	8.3	24.08.2012	82.96	1.447	2.692	46.2
21A	6.6	31.08.2012	42.37	-	-	-
22	-	16.12.2012	59.37	-	-	-
23	8.4	17.12.2012	306.97	-	-	-
24	6.5	20.12.2012	5.85	-	-	-
25	6.5	21.12.2012	28.05	-	-	-
26	6.5	23.12.2012	16.83	-	-	-
27	6.5	17.03.2013	107.16	-	-	-
28	6.5	24.04.2013	321.74	-	-	-
29	6.5	10.05.2013	278.61	-	-	-

D is the distance from the crater measured in km. Towns can be tracked at figure 1.

(*e.g.*, Heiken and Wohletz, 1985; Sherdian and Marshall, 1983; Wholetz, 1986; Dellino and Kyriakopoulos, 2003). The SEM analyses were carried out using a Tescan-Vega (Bruker) instrument operating at 15.0 kV. The ash grains, previously selected under the binocular microscope, were placed inside a circular slide (1 cm diameter) on double-sided coal tape, as suggested by Lautze *et al.,* 2012. The samples were coated with a thin metallic layer (200A gold in 20 seconds) prior to analysis in the SEM.

3.3. Grain size

Tephra was mechanically sieved from 63 to 2,000 μm (-1 to 4Φ) at regular steps of 0.5Φ ($\Phi=-\log_2 D/D_0$, with D being the particle diameter and D_0 a reference diameter as 1 mm), using a Fritsch analysette instrument, during a period of 3-5 minutes in order to avoid the over-fracturing of tephra. Respective grain size fractions were weighted and their mass fraction (wt%) was determined using the total mass of each sample. The sample statistics (M_d=median; M_z=mean; σ_1=sorting or standard deviation; S_k=skewness; K_G=kurtosis) were then calculated using the Gradisat package (Blott and Pye, 2001) which uses the Method of Moments in Microsoft Visual Basic programming language. Linear interpolation is used to calculate statistical parameters by the Folk and Ward (1957) graphical method, and to derive physical descriptions (such as "very coarse sand" and "moderately sorted") (Blott and Pye, 2001). We also compared these descriptions with the classification of Cas and Wright (1987) which is commonly used for the study of volcanic deposits. After measuring the <63 μm (4Φ) ash fraction, we used the method of Horwell (2007) to estimate both "thoracic" (<10 μm; 6.7Φ) and "respirable" (<4 μm; 8Φ) ash amounts particles.

3.4. Chemistry and mineralogy

The major element chemical characterization of bulk ash (particles finer than 4Φ) samples was analyzed by Energy Dispersion Spectrometer (EDS) for SEM with a Qantax EDS (Bruker instrument). The procedure consisted in the mapping and averaging of 100 points in order to avoid heterogeneity effects from individual particles. These particles were not separated prior geochemical analyses, thus the results from samples exclusively compound by fresh juvenile particles are discussed. Work distance was 26 mm, with Secondary Electron Detector (SE) and the software Spirit 1.8 with a detection limit of 1% for the recognized elements.

Mineralogy was characterized from pulverized samples of ash (particles finer than 5Φ) at the X-Ray diffractometer (XRD) D8-Advance. The qualitative and quantitative identification of mineral phases were carried out with the software Diffrac^{plus} (EVA) and these phases were compared with the XRD spectrums of the International Center of Diffraction Data (ICDD) database. In the case of minerals with continue compositions (*e.g.,* plagioclases, from albite to anorthite) these are named as the amount of one of these two end-members changes (*e.g.,* anorthite), producing different X-Ray powdered diffraction patterns and intensities (*e.g.,* Goodyear and Duffin, 1954). Additionally, a semi-quantitative analysis of amorphous material was done with Topas 4.2 software.

4. Results

4.1. Lithological and textural characteristics of tephra

Based in lithology, we have distinguished five types of particles within the tephra samples.

4.1.1. Scoria

It can be dark (black), brown or reddish. Black scoria (Fig. 3A) correspond to dark, sometimes glassy particles, generally with vesicles. Brown scoria is a transparent or semi-transparent (glassy) brown material with vesicles (Fig. 3A). Reddish scorias are subrounded to sub-angular vesiculated particles altered by hidrothermal processes (Fig. 3B).

4.1.2. Pumice

Particle of a clear to intermediate gray-color, highly vesicular glassy material whose vesicles are sub-spherical (Fig. 3C).

4.1.3. Lithics

lithics correspond to dense angular rocks fragments, black or reddish in color, blocky, porphyritic or microcrystalline and non-vesicular (Fig. 3D). Even if part of these particles might be juvenile, they are considered as lithics because they were crystallized pior to their fragmentation (in older lavas or hipabisal intrusions).

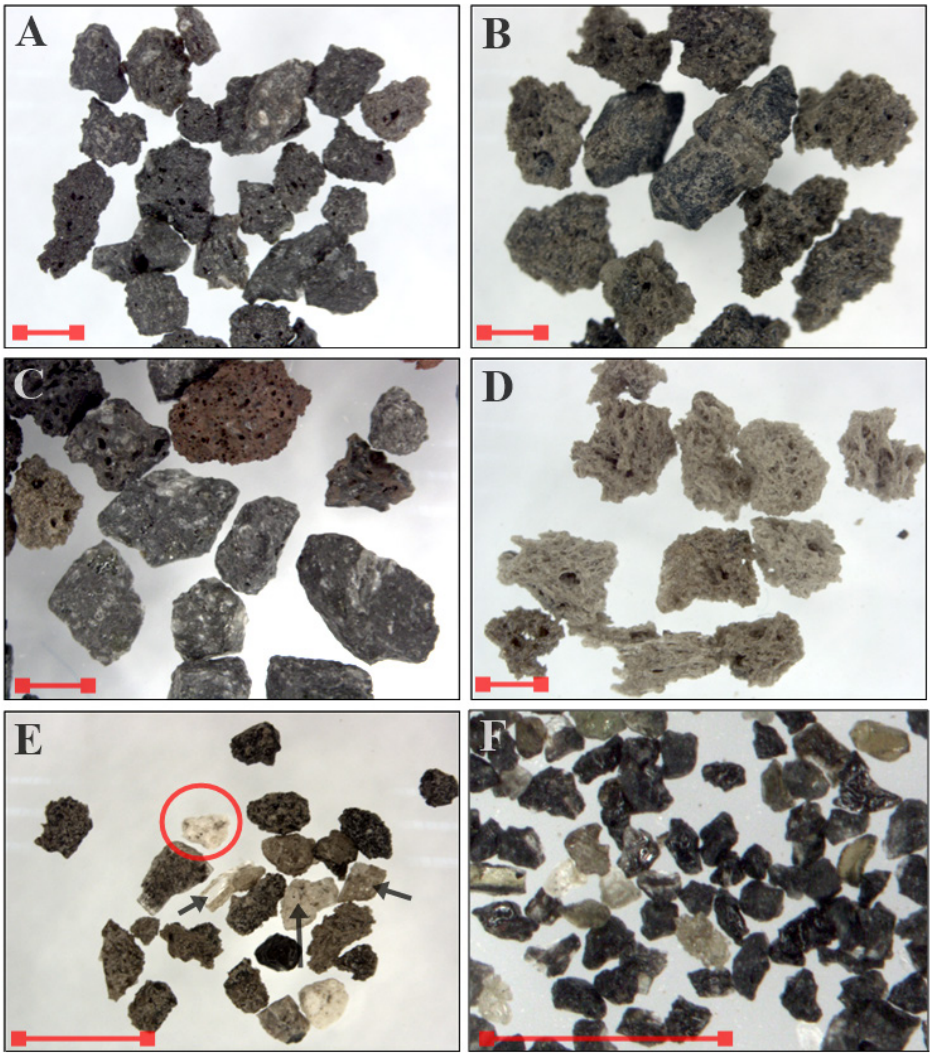

FIG. 3. Lithologic components identified by optical microscope in ash samples from Tungurahua. **A.** Black scoria fragment in sample 5; **B.** Brown scoria in sample 9B; **C.** Reddish scoria and lithics found in sample 19A; **D.** Pumice particles with elongated vesicles from sample 13; **E.** Free crystals (mainly plagioclase, black arrows) found in sample 17. Also, an aggregate is highlighted with a red circle; **F.** Glass shards in sample 8. For scale purposes, red bars are 1 mm in length.

4.1.4. Crystals

Free crystals are sub-rounded and idiomorphic fragments (Fig. 3E).

4.1.5 Glass shards

Glass shards are transparent to semi-transparent, uncolored or clear brown, dense and non-vesicular material (Fig. 3F). Sharp perimeters and conchoidal fractures are typically observed. White spherical aggregates of finer fragments are ocassionally found (Fig. 3E).

Thus, we considerate as fresh juvenile constituents of tephra only scoria, pumice, free crystals and glass shards as they directly result from the primarly magma fragmentation. In contrast, lithics and altered fragments such as reddish scoria are interpreted to be accidental.

Quantitative variations of these components are reported in figure 4. Also, we qualitatively describe the juvenile (mostly glassy) particles in function of their morphology (vesicularity, shape and surface; Fig. 5) as follows:

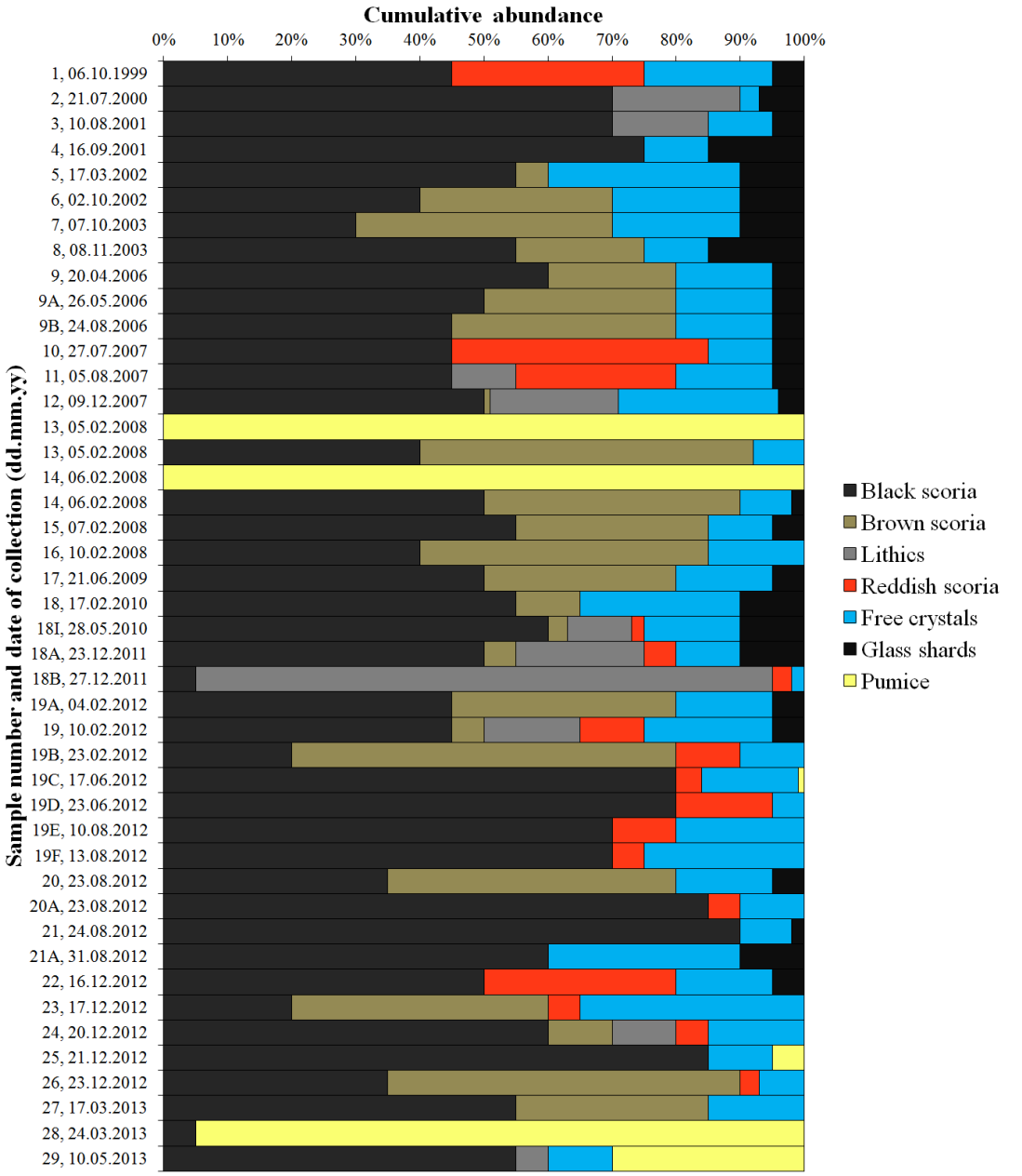

FIG. 4. Relative proportion of the different components of tephra samples of eruptions between 1999 and 2012 at Tungurahua volcano.

4.1.6. Apparent vesicularity

The amount (%) of vesicles is optically estimated within the selected particles. We classify particles as none vesicular (0%; Fig. 5A1), lowly vesicular (1-25%; Fig. 5B1), moderately vesicular (26-50%; Fig. 5C1) and highly vesicular (>50%; Fig. 5D1).

4.1.7. Shape

The particles are grouped into four categories: **1)** IVW or inter-vesicular walls (Fig. 5A2), **2)** fluid (spheric or tear-shaped glassy droplets; Fig. 5B2), **3)** filamentous (very elongated particles, such as Peleé tears or fibers; Fig. 5C2) and **4)** blocky particles (generally compact and porous grains; Fig. 5D2).

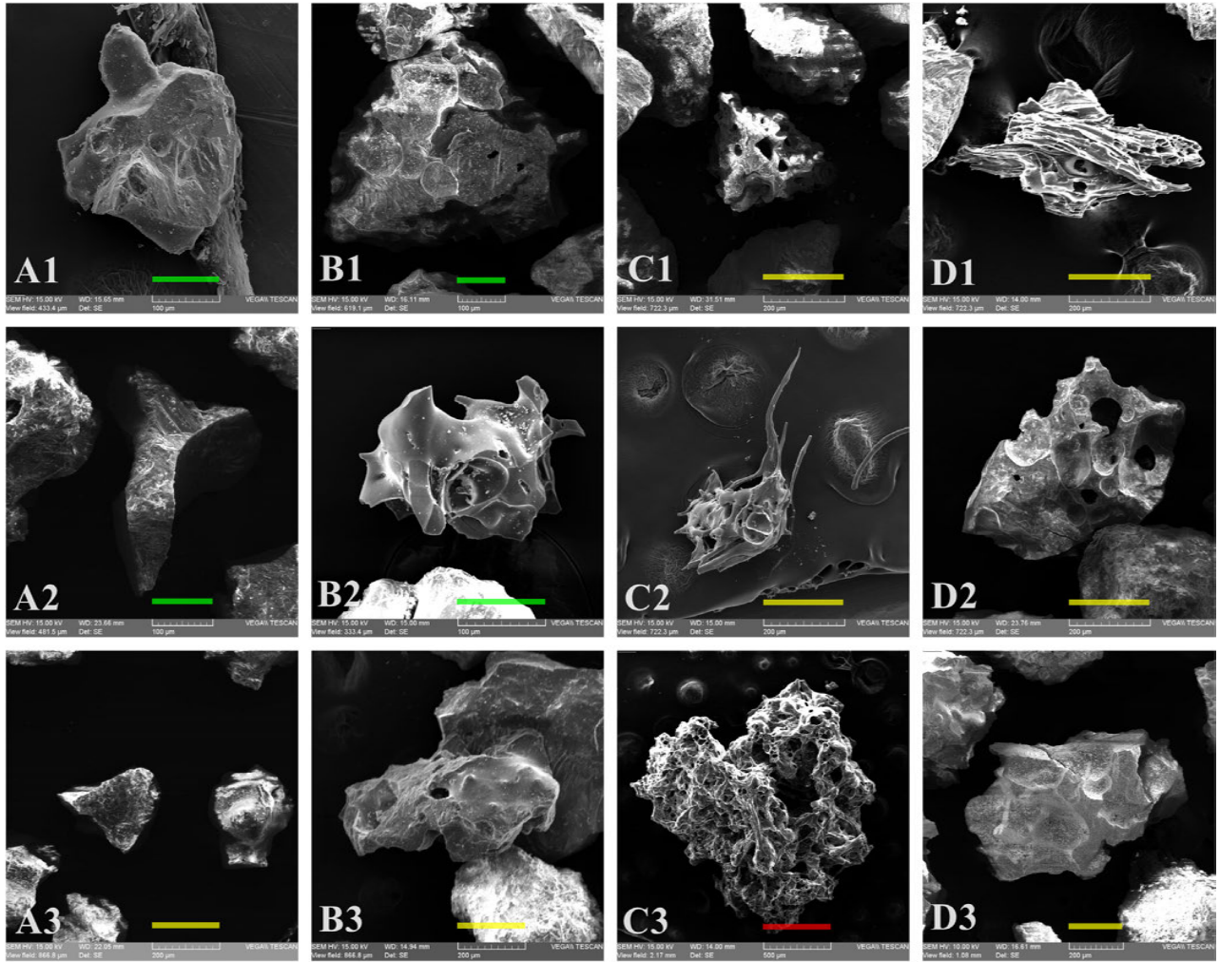

FIG. 5. Qualitative characterization of juvenile ash particles using SEM-EDS in function of their vesicularity (from A1 to D1), shape (from A2 to D2) and surface/perimeter (from A3 to D3). **A1**: Sample 19; **B1**: Sample 6; **C1**: Sample 1; **D1**: Sample 13; **A2**: Sample 5; **B2**: Sample 19A; **C2**: Sample 13; **D2**: Sample 4; **A3**: Sample 5; **B3**: Sample 9; **C3**: Sample 13; **D3**: Sample 20. For sample details please refer to table 1 and figure 1. Scale bars correspond to 100 µm (green), 200 µm (yellow) and 500 µm (red).

4.1.8. Surface or perimeter

This category includes: **1)** smoothed particles (Fig. 5A3), **2)** molten surfaces (mild, bulbous and waken particle faces; Fig. 5B3), **3)** jagged perimeters (as product of abundant blowed up vesicles; Fig. 5C3) and **4)** broken grains as product of recycling of older pyroclasts (Fig. 5D3).

4.2. Lithological and textural variations of tephra through time

4.2.1. Phase I

The first tephra sample collected in October 1999 was dominantly compound of black scoria (45%), with a large proportion of altered reddish scoria (30%), free crystals (20%) and scarce glass shards (5%) (Fig. 4). Glassy particles were moderately vesicular, with jagged perimeter. Subsequent ash emissions up to 2001 ejected increasing black scoria (70-75%), lithics (0-20%), free crystals (5-10%) and increasing glass shards (5-15%) (Fig.4) suggesting more participation of juvenile magma. These glassy particles had low vesicularity and blocky shapes (Table 2). Between 2002 and 2003 the ash was compound of dominant black scoria (30-55%), brown scoria (5-40%), decreasing amounts of free crystals (10-30%) and relative stable amounts of glass shards (10-15%) (Fig. 4). These glassy particles had none-to-low in vesicularity, shaped as inter-vesicular walls and their perimeter was smoothed or molten (Table 2).

4.2.2. Phase II

In Phase II, black scoria, brown scoria, free crystals and glass shards were observed. Since April 2006 and up to August 2006, the amount of black scoria decreased from 60 to 45%, while the participation of brown scoria increased from 20 to 35% (Fig. 4). The free crystals remained constant in time (15%) as similarly to glass shards (5%) (Fig. 4). Glassy particles collected in 2006 (before the August 2006 eruption) had none, low or moderate vesicularity (vesicles were, in most of cases sub-spherical), with blocky shape and broken or jagged perimeters (very scarce molten perimeters) (Table 2). After the paroxysmal eruption of 16 August 2006, the morphology of ash grains evolved in 24 August to moderately or highly vesicular (vesicles were subrounded or slightly elongated), with blocky shapes and the perimeters of these particles were smoothed, molten and jagged (Table 2).

4.2.3. Phase III

Within the 2007 ash samples there was a new incursion of altered scoria and lithics (30-45% and 10-20% respectively), even when these samples are also dominated by 45-50% black scoria, 10-25% free crystals and about 5% glass shards, with very small amounts of brown scoria (1-2%) (Fig. 4). The glassy particles were not vesicular or moderately vesicular, with blocky shape and smoothed and molten perimeters (Table 2). Two samples collected by 5-6 February 2008 were exclusively compound of pumice, which had low to high vesicularity, fluid and filamentous shapes and molten or jagged perimeters (Fig. 4). Their vesicles were subrounded to elongated, forming “tubes”. Hereafter the tephra emissions ejected increasing amounts of black scoria (50-60%), increasing free crystals (7-20%), increasing glass shards (<5 to 10%) and decreasing brown scoria (<5 to 40%) up to Feruary 2010 (Fig. 4). Glassy particles were low to moderately vesicular, blocky shaped and with smoothed, molten and jagged perimeters (Table 2).

4.2.4. Phase IV

The components of the ashes since 2010 up to 2013 show chaotic patterns in time if compared to the pre-2010 eruptions. In fact, glass shards (<5 to 10%), altered scoria (<5 to 30%), brown scoria (10-45%) and lithics (10-90%) are sporadically present (Fig. 4). Black scoria remains always present but in varying proportion (50-90%), similarly to free crystals (<10 to 30%) (Fig. 4). The glassy particles were not vesicular or exhibited moderate-to-high vesicularity, a widespread variety of shapes (fluid, filamentous and blocky) with smoothed and broken perimeters (Table 2). A noticeable change occurs since December 2012 when glass shards are not longer observed (Fig. 4). However, the morphology of glassy particles (scoria and pumice) revealed to be low-to-moderate in vesicularity with molten and broken perimeters (Table 2). Also, relevant amounts (25-95%) of pumice are observed within the samples collected in March and May 2013 (Fig. 4).

4.3. Grain size

We observed unimodal (Fig. 6A; 11.9%), bimodal (Fig. 6B; 76.2%) and trimodal (Fig. 6C; 11.9%) grain size distributions (GSD) within the tephra samples (Table 3). Between 1999 and 2009, deposits

TABLE 2. SYNTHESIS OF TEXTURE AND STRUCTURE OBSERVED ON JUVENILE PARTICLES ERUPTED BY TUNGURAHUA BETWEEN 1999 AND 2013 USING SEM-EDS.

Sample	Date	Glassy particles											
		Vesicularity				Shape				Surface /perimeter			
		none	low	moderate	high	IVW*	fluid	filamentous	blocky	smoothed	molten	jagged	broken
1	06.10.1999			■								■	
2	21.07.2000		■						■				
3	10.08.2001		■						■				
4	16.09.2001		■						■				
5	17.03.2002	■				■				■	■		
6	02.10.2002		■										
9	20.04.2006	■							■		■	■	■
9A	26.05.2006	■	■	■		■			■	■			
9B	24.08.2006	■		■	■				■	■	■	■	
10	27.07.2007			■					■	■			
11	05.08.2007	■							■				
12	09.12.2007	■					■		■		■		■
13	05.02.2008			■	■		■	■	■			■	
14	06.02.2008		■					■	■		■		
15	07.02.2008			■					■			■	
18	17.02.2010		■	■					■	■	■		
18 I	28.05.2010			■	■			■	■	■			■
19 A	04.02.2012			■			■						
19	10.02.2012	■								■			
20	23.08.2012			■							■		■
21	24.08.2012		■	■							■		

Shading positions indicate the occurrence of the respective textural feature.
IVW* correspond to inter-vesicular walls.

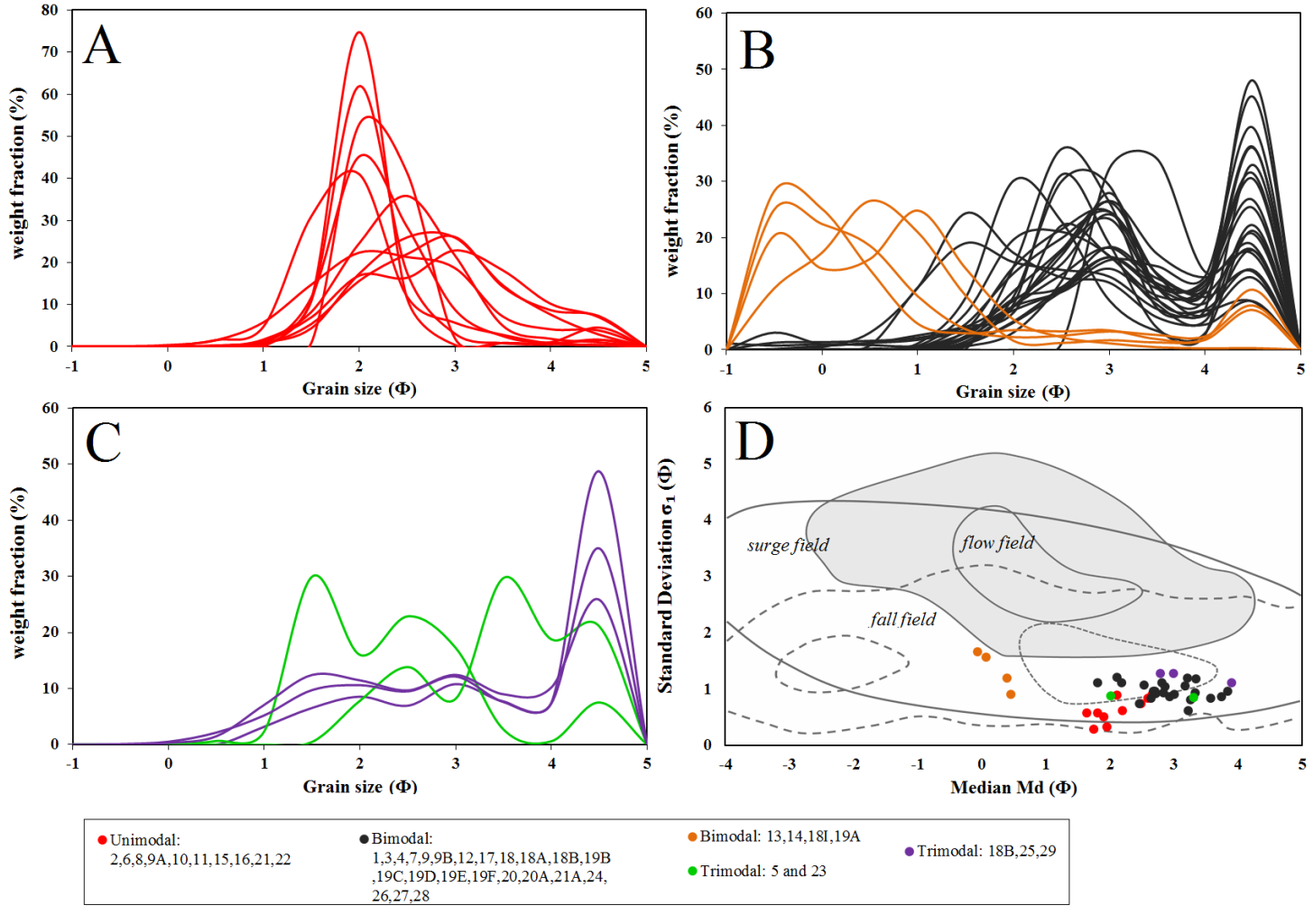

FIG. 6. Grain size distribution (GSD) of tephra fall samples. **A.** Unimodal GSD (red); **B.** Bimodal GSDs, where two main bimodal populations are recognized (orange and dark grey); **C.** Trimodal GSD with also two main populations (green and violet); **D.** Walker (1971) classification for GSD of pyroclastic deposits. The samples here studied plot in the field of fall deposits. Colours from lines and circles correspond to each cluster of unimodal or polymodal samples.

TABLE 3. GRAIN SIZE PARAMETERS OF FOLK AND WARD (1957) FOR 42 SAMPLES SIEVED MECHANICALLY.

Sample	Folk and Ward (1957) statistics (Φ)						Modes			Fine to extremely fine ash		
	Md	Mz	σ1	Sk	KG	S	M1	M2	M3	<63 µm	<10 µma	<4 µmb
1	2.87	3.02	1.04	0.06	0.76	P	4.23	2.24	-	25.29	6.55	2.11
2	2.11	2.12	0.89	0.07	1.08	M	2.24	-	-	3.85	0.92	0.19
3	2.94	3.05	0.86	0.11	0.87	M	2.74	4.23	-	17.08	4.29	1.2
4	1.82	2.03	1.1	0.3	0.98	P	1.25	4.23	-	8.66	2.11	0.49
5	3.31	3.23	0.85	-0.16	0.86	M	3.24	4.23	2.24	21.1	5.38	1.62
6	1.96	1.98	0.32	0.08	0.74	VW	1.75	-	-	1.58	0.38	0.07
7	3.23	3.34	0.61	0.23	0.83	MW	3.24	4.23	-	18.68	4.72	1.36
8	2.2	2.21	0.61	0.02	1.09	MW	2.24	-	-	1.03	0.24	0.05
9	2.46	2.64	0.74	0.37	1.26	M	2.24	4.23	-	8.58	2.09	0.49
9A	2.6	2.63	0.83	0.09	1.02	M	2.74	-	-	7.3	1.77	0.4
9B	2.81	2.89	1.11	-0.03	1.04	P	2.74	4.23	-	17.81	4.49	1.27
10	1.81	1.88	0.58	0.4	2.33	MW	1.75	-	-	4.54	1.09	0.23
11	1.65	1.67	0.58	0.14	1.27	MW	1.75	-	-	0.31	0.07	0.01
12	3.58	3.44	0.84	-0.29	0.73	M	4.23	3.24	-	39.61	10.76	4.21
13	0.4	0.49	1.18	0.34	1.87	P	0.25	4.23	-	7.08	1.72	0.38
14	0.07	0.63	1.56	0.58	1.42	P	-0.74	4.23	-	7.88	1.92	0.44
15	2.5	2.53	0.74	0.09	1.03	M	2.24	-	-	2.91	0.69	0.14
16	2.66	2.64	0.89	-0.01	0.92	M	2.74	-	-	7.03	1.7	0.38
17	3.17	3.13	1.05	-0.15	0.79	P	4.23	2.74	-	30.47	8.03	2.8
18	2.69	2.88	0.95	0.22	0.89	M	2.74	4.23	-	17.72	4.46	1.26
18I	-0.07	0.67	1.66	0.65	1.05	P	-0.74	4.23	-	10.71	2.63	0.64
18A	2.11	2.31	1.2	0.22	0.85	P	1.25	4.23	-	12.85	3.18	0.82
18B	2.79	2.75	1.28	-0.09	0.64	P	4.23	1.25	2.74	25.84	6.7	2.18
19A	0.46	0.38	0.89	-0.04	0.88	M	0.75	-0.74	-	0.29	0.07	0.01
19	3.35	3.12	1.17	-0.34	0.77	P	4.23	2.74	-	37.18	10.02	0.59
19B	3.26	3.33	0.8	0.05	0.65	M	4.23	2.74	-	36.01	9.67	0.57
19C	3.01	3.13	0.9	0.11	0.68	M	4.23	2.74	-	26.7	6.94	0.38
19D	2.65	2.87	0.83	0.33	1	M	2.24	4.23	-	14.22	3.54	0.17
19E	3.75	3.49	0.85	-0.44	0.7	M	4.23	2.74	-	45.13	12.48	0.79
19F	3.34	3.27	0.92	-0.16	0.69	M	4.23	2.74	-	36.2	9.72	0.57
20	3.85	3.46	0.95	-0.57	0.72	M	4.23	2.74	-	48.03	13.41	0.86
20A	2.72	2.83	0.92	0.15	0.91	M	2.74	4.23	-	13.93	3.46	0.17
21	1.91	1.96	0.5	0.18	1.15	MW	1.75	-	-	1.66	0.4	0.08
21A	2.85	3	0.93	0.16	0.8	M	2.74	4.23	-	20.7	5.27	1.58
22	1.76	1.76	0.29	0.03	1.39	VW	1.75	-	-	0.44	0.1	0.02
23	2.02	2.03	0.88	0.19	1.06	M	1.25	2.24	4.23	7.53	1.83	0.41
24	2.54	2.8	1.06	0.26	0.71	P	4.23	2.24	-	22.22	5.69	1.75
25	3.9	3.36	1.11	-0.67	0.76	P	4.23	2.74	1.75	48.73	13.64	5.9
26	2.71	3.01	0.95	0.33	0.6	M	4.23	2.24	-	32.98	8.76	3.16
27	2.19	2.63	1.11	0.45	0.8	P	1.75	4.23	-	21.2	5.41	1.63
28	3.21	3.11	1.19	-0.27	0.93	P	4.23	2.74	-	31.46	8.32	2.94
29	3	2.89	1.27	-0.18	0.66	P	4.23	2.74	1.75	35.01	9.36	3.47

Md: median; **Mz:** mean; **σ1:** sorting; **Sk:** skewness; **KG:** Kurtosis. For sample distribution modes 1, 2 and 3 are M1, M2 and M3. Also, for sample sorting (**S**) the label meaning is defined as follows: **P:** poorly sorted, **M:** moderately sorted; **W:** Well sorted and **VW:** Very well sorted. **a.** Calculated using the method (1) of Horwell (2007): y=0.0009x2+ 0.236x, where y is the cumulative% <10 µm and x is the cumulative% <63 µm fraction. **b.** Calculated using the method (2) of Horwell (2007): y=0.0016x2+ 0.043x, where y is the cumulative% <4 µm and x is the cumulative% <63 µm fraction. The correlation (R2) of methods (1) and (2) are 0.853 and 0.88, respectively. The bold data correspond to the three highest values of finest ash fraction of all the samples.

with unimodal and bimodal GSD's were frequently interspersed, but from 2009 to 2012 most of the samples had a bimodal or trimodal distribution. The tephra from the August 2006 eruptions is bimodal, with modes at 2.74 and 4.23Φ (medium to very fine ash). The trimodal GSD's are typical of samples from the 2002, 2011, 2012, and 2013 eruptions. According to the classification of Folk and Ward (1957), 37% of the samples are poorly sorted, 50% are moderately sorted, 12.5% are moderately well sorted and 5% are very well sorted (Table 3). The classification of Cas and Wright (1987) is currently the most used for volcanic deposits, and with their criteria 62.5% of the samples are very well sorted and 12.5% are well sorted. In general, average values of M_d=2.48Φ (medium to fine ash), M_z=2.54Φ (medium to fine ash), σ_1=0.93 (well sorted)Φ S_k=0.07Φ (asymmetrically positive) and K_G= 0.96Φ are observed for the whole dataset (Table 3). All samples are well classified as fall deposits according to the scheme of Walker (1973) (Fig. 6D).

The abundance of particles smaller than 4Φ varied from 0.3 to 48 wt% of the total ash samples, and frequently (~21%) it is <5 wt% (Table 3). Nevertheless, in other cases (~12%) this fraction accumulates 35-40 wt%. Samples with the highest content of <4Φ ash (35-50 wt%) were erupted in August 10th, August 23rd and December 21st 2012, while other samples erupted in December 2007, February and August 2012 had also high amounts of fine ash (Table 3). In contrast, the lower amounts of ash finer than 4Φ were found during the eruptions of July and October 2002, July and August 2007, February 2009, February 2012 and August and December 2012 (samples 2, 6, 8, 10, 11, 15, 19A, 21, and 22). Sample 9B (August 24th 2006) has an intermediate amount of fine ash (15-20%) (Table 3).

The particles smaller than 6.7Φ ranged from 0.07 to 13.64 wt% in all samples, with an average of 4.9 wt%, and the <8Φ fraction ranged from 0.01 to 5.9 wt% with an average of 1.14 wt% (Table 3).

4.4. Bulk ash geochemistry

Due to the coexistence of different particle classes together in ash (including lithics and altered particles), only 21 of 43 geochemical analyses are considered as useful for describing the bulk geochemistry erupted materials, as they are exclusively compound by fresh juvenile particles (scoria, pumice, glass shards and free crystals) as shown in table 4. According to the total alkali-silica (TAS; Le Maitre, 1984) classification scheme (Fig. 7A), the samples from the whole eruptive style (Table 3) plot in the andesite compositional field, with a SiO_2 range between 57.9 and 62.3 wt%.

Harker diagrams are shown in figure 7B-H. Linear trends are only identified in FeO, CaO, and K_2O *versus* SiO_2 variation diagrams, while a major scattering is observed in TiO_2, Al_2O_3 and MgO contents. In general, samples collected in 2012-2013 are slighly enriched in CaO and K_2O (Fig. 7F and 7H), but depleted in MgO and Na_2O (Fig. 7E and 7G) if they are compared with the samples that represent the 2001-2010 eruptions. CaO *versus* MgO (Fig. 7I), molar K_2O/K_2O+CaO *versus* MgO (Fig. 7J) and the pseudoternary system defined by Opx-An-Or (Fig. 7K) (Díaz-Alvarado *et al*., 2011; Castro, 2013) are particularly significant for visualizing linear trends in co-genetic igneous rocks. However, Tungurahua samples display a significant scattering for a scarce SiO_2 variation. The higher CaO and K_2O and lower MgO contents observed in the 2012-2013 samples regarding to the rest of the studied ash deposits separate two groups of samples in these diagrams.

4.5. Mineralogy

The ash mineralogy is characterized by the assemblage of plagioclase (plg; 58.4%), pyroxene (px; 37.00%) of both clinopyroxene (cpx; 29.98%) and orthopyroxene (opx; 7.04%) classes, olivine (ol; 3.38%), and 1.40% of akermanite (ak) and magnetite (mag) (Table 5).

The recognized plagioclases corresponded to anorthite (16-31%), andesine (13-22%) and albite (9-21%). The plg was generally observed in the ash samples (53-65%), and its maximum relative proportion is found in the 2006 samples (62-65%). Pyroxenes consist of both cpx and opx. The cpx was identified as diopside (9-20%), pigeonite (7-18%) and, in a few cases, of hedenbergite (1-3%). On other hand, the only estantite was recognized for opx (3-12%). In general, the highest proportions of px were found in ash samples from 2001 and 2002 eruptions (Table 5; 41-44%). Olivine was forsteritic, varying from 2 to 9% and with its highest relative proportion in the samples of year 2003 (sample 7). As accessory minerals, akermanite and magnetite were found (Table 5). Akermanite varied from 1-2%,

TABLE 4. BULK ASH MAJOR ELEMENT CHEMICAL COMPOSITION FOR THE SAMPLES OF TUNGURAHUA VOLCANO COMPOUND EXCLUSIVELY BY JUVENILE PARTICLES, FROM ERUPTION OCCURRED BETWEEN 1999 AND 2013.

Sample	Oxide (wt%)								
	SiO_2	Al_2O_3	FeO	CaO	MgO	Na_2O	K_2O	TiO_2	Total
4	57.87	16.55	8.01	8.42	3.33	3.56	1.45	0.78	99.98
5	60.16	17.19	6.69	7.04	2.27	3.55	2.14	0.98	100.02
6	59.82	15.34	7.85	7	3.5	3.59	2.08	0.82	99.99
7	59.64	15.68	8.12	7.18	3	3.84	1.61	0.92	100
8	58.9	15.53	7.98	8.02	3.65	3.57	1.54	0.8	99.98
9A	58.49	15.36	8.66	7.86	3.56	3.64	1.69	0.75	100.01
9B	62.28	14.04	7.87	7.16	2.79	3.41	1.77	0.67	99.99
13	57.98	15.44	9.22	7.6	3.48	3.34	1.95	0.98	99.99
14	58.85	15.27	8.08	7.42	3.43	3.55	2.43	0.97	99.99
15	60.76	15.19	7.06	7.25	2.72	3.91	2.35	0.75	99.99
16	59.47	16.44	7.51	7.74	2.49	3.65	1.83	0.85	99.98
17	58.19	16	7.99	8.13	3.07	3.55	2.2	0.9	100.03
18	58	16.82	7.9	8.05	3.02	3.4	2.06	0.75	99.98
19A	59.58	15.61	7.06	7.88	3.28	3.64	2.25	0.68	99.99
20	60.35	15.53	7.2	7.39	2.55	3.75	2.52	0.68	99.98
21	59.6	15.36	7.6	7.72	3.18	3.56	2.14	0.82	99.99
21A	58.77	16.14	8.3	8.3	2.72	2.82	2.22	0.78	100.03
25	59.07	16.06	8.32	8.6	2.24	2.57	2.29	0.83	99.99
27	59.15	15.98	8.5	8.41	2.21	2.83	2.2	0.75	100.04
28	59.62	16.17	8.48	8.33	2.11	2.31	2.36	0.67	100.04
29	60.03	16.5	7.29	8.09	2.12	2.74	2.54	0.68	99.99

and its highest relative proportion occurs in 2006 ash samples, though it was also found in 2008, 2010, 2011, and 2012 samples. The magnetite is in the range from 1 to 3% (3% in the 2012 ash).

5. Discussion

5.1. Eruption mechanisms and style transition between 1999-2013

5.1.1. Phase I

The vent-cleaning phase of reawakening at Tungurahua in 1999 (Ruiz *et al.,* 2006; Le Pennec *et al.,* 2012) was recorded within the first tephra fall sample (October 1999) which involved a notable proportion of hydrothermally altered scoria (30%) and small amounts (5%) of glass shards. The recognizance of hydrothermal alteration at juvenile particles is a good tool to assess the existence of juvenile material recycling (*e.g.,* Houghton and Smith, 1993). These particles are expected to contribute little, if any, thermal energy to the explosions (Hougton and Carey, 2015). The jagged perimeter of some of these particles indicates a brittle fragmentation, thus probably of pre-existent deposits. There were not observed particles with quenching cracks, commonly associated to the fast passage (a few milliseconds) of newly fragmented particles through a domain of liquid water (Büttner *et al.*, 1999), thus a phreatomagmatic origin is unlikely. However, there are inherent limitations of particle observation associated to the grain size fractions here studied, thus that phreatomagmatic should not be totally discarded, and both lithologic and textural patterns here observed have been frequently associated to the initial phreatic-phreatomagmatic transitional stages of volcano reawakening, such

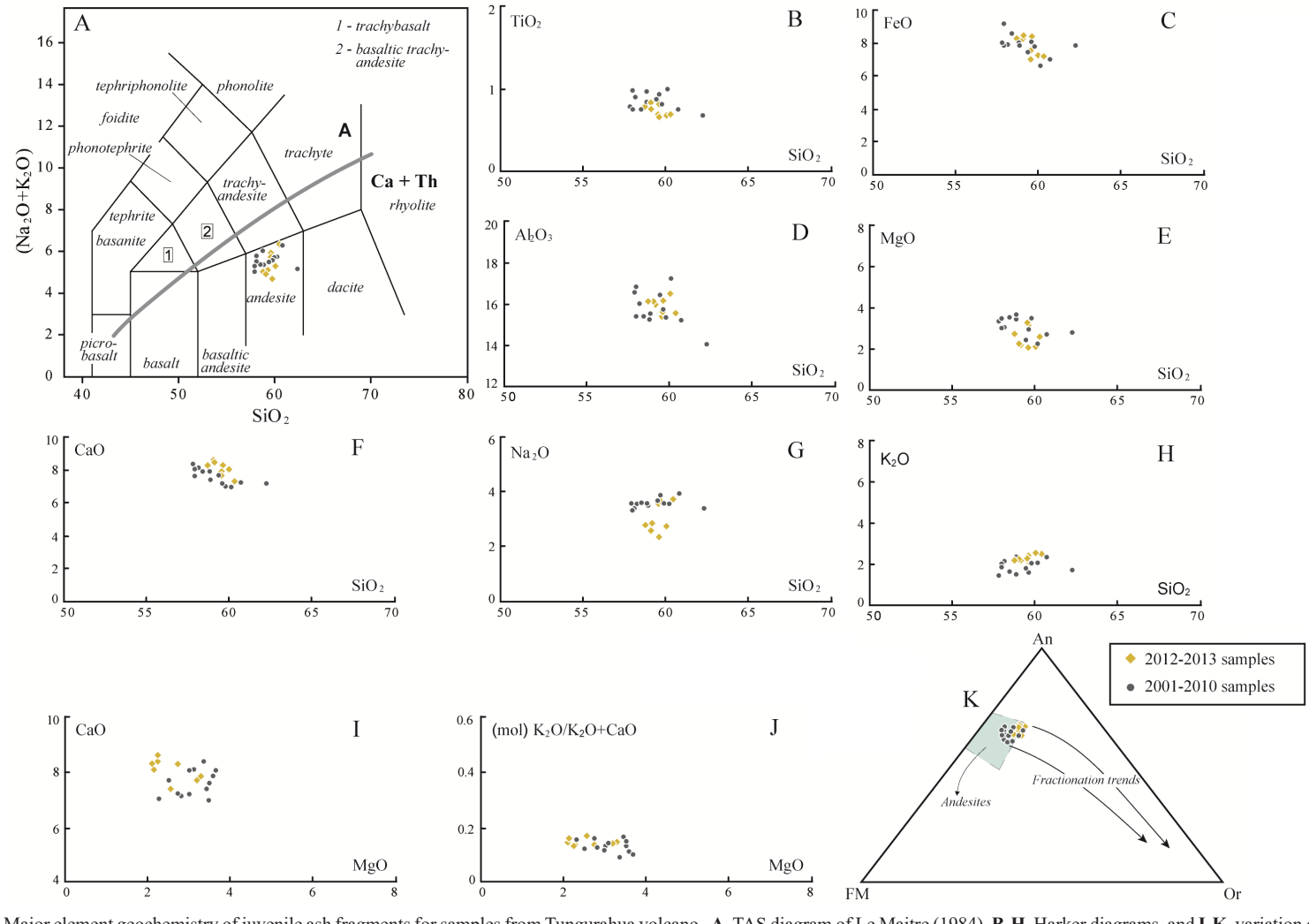

FIG. 7. Major element geochemistry of juvenile ash fragments for samples from Tungurahua volcano. **A.** TAS diagram of Le Maitre (1984). **B-H.** Harker diagrams, and **I-K.** variation diagrams. In A: A alkaline, Ca+T Calcoalkaline+Tholeiitic; In K: FM Ferromagnesian minerals (Fe-Mn-Mg), An Anorthite, Or Orthoclase.

TABLE 5. MINERALOGICAL COMPOSITION OF ASH SAMPLES COLLECTED BETWEEN 1999 AND 2013 AT TUNGURAHUA VOLCANO. ALL THE ABUNDANCES ARE MODAL%.

	Mineral, % abundance												
	Plagioclase group				Pyroxene group					Other			
Mineral	Anortite	Andesine	Albite	Amount	Diopside	Pigeonite	Hedenbergite	Enstatite	Amount	Olivine	Akermanite	Magnetite	Total
Formula	$CaAl_2Si_2O_8$	$(Na,Ca)(Al,Si)_2Si_2O_8$	$NaAlSi_3O_8$		$Ca(Mg,Al)(Si,Al)_2O_6$	$(Mg,Fe,Ca)SiO_3$	$CaFeSi_2O_6$	$MgSiO_3$		$(Mg,Fe)_2SiO_4$	$Ca_2MgSi_2O_7$	Fe_3O_4	
1	25	18	16	59	14	15	-	8	37	4	-	-	100
2	24	17	16	57	12	16	-	10	38	5	-	-	100
3	24	16	14	54	16	15	1	12	44	2	-	-	100
4	21	15	17	53	14	18	1	9	42	5	-	-	100
5	24	17	15	56	15	15	-	11	41	3	-	-	100
6	25	15	14	54	20	7	1	16	44	2	-	-	100
7	20	21	12	53	15	16	-	7	38	9	-	-	100
8	22	17	18	57	18	16	1	6	41	2	-	-	100
8A	26	18	20	64	11	18	1	3	33	3	-	-	100
9	25	22	15	62	15	14	-	4	33	3	2	-	100
9A	25	18	20	63	9	18	2	3	32	2	2	1	100
9B	31	16	18	65	12	14	1	6	33	-	1	1	100
10	25	21	12	58	14	12	2	9	37	5	-	-	100
11	27	19	9	55	15	17	1	6	39	5	-	1	100
12	23	16	17	56	14	15	2	7	38	4	1	1	100
13	27	13	18	58	11	15	2	8	36	3	2	1	100
14	28	15	15	58	12	16	3	7	38	3	-	1	100
15	23	15	21	59	13	15	2	6	36	4	1	-	100
16	23	20	17	60	12	16	-	8	36	2	2	-	100
17	23	20	16	59	15	12	2	6	35	4	-	2	100
18	28	18	16	62	11	16	2	5	34	4	-	-	100
18 I	25	19	17	61	14	12	3	5	34	4	-	1	100
18A	16	19	25	60	10	17	2	9	38	2	-	-	100
18B	26	16	16	58	15	12	2	9	38	3	1	-	100

table 5 continued.

	Mineral,% abundance												
	Plagioclase group				Pyroxene group					Other			
Mineral	**Anortite**	**Andesine**	**Albite**	**Amount**	**Diopside**	**Pigeonite**	**Hedenbergite**	**Enstatite**	**Amount**	**Olivine**	**Akermanite**	**Magnetite**	**Total**
Formula	$CaAl_2Si_2O_8$	$(Na,Ca)(Al,Si)_2Si_2O_8$	$NaAlSi_3O_8$		$Ca(Mg,Al)(Si,Al)_2O_6$	$(Mg,Fe,Ca)SiO_3$	$CaFeSi_2O_6$	$MgSiO_3$		$(Mg,Fe)_2SiO_4$	$Ca_2MgSi_2O_7$	Fe_3O_4	
19A	28	16	12	56	12	18	3	4	37	5	2	-	100
19	19	17	18	54	15	11	3	11	40	2	1	3	100
19B	29	20	15	64	19	7	2	5	33	2	1	-	100
19C	27	19	14	60	16	13	2	6	37	2	-	1	100
19D	17	18	23	58	23	5	2	7	37	3	-	2	100
19E	29	19	12	60	11	14	3	7	35	3	2	-	100
19F	28	18	12	58	13	14	5	6	38	2	2	-	100
20	31	18	14	63	14	7	2	7	30	5	1	1	100
20A	22	23	13	58	14	17	2	4	37	4	-	1	100
21	20	19	17	56	16	17	1	5	39	3	-	2	100
21A	28	22	6	56	15	18	1	7	41	2	-	1	100
22	23	14	23	60	22	6	1	6	35	2	1	2	100
23	27	18	13	58	12	20	3	4	39	2	1	-	100
24	28	15	20	63	11	9	1	9	30	5	1	1	100
25	23	20	15	58	9	13	3	8	33	5	2	2	100
26	24	18	17	59	17	11	3	8	39	2	-	-	100
27	23	19	13	55	21	14	2	5	42	3	-	-	100
28	20	16	18	54	16	12	3	7	38	5	1	2	100
29	27	18	15	60	12	15	3	7	37	2	1	-	100

as the case of Cotopaxi in 2015 (*e.g.,* Gaunt *et al.*, 2016; Troncoso *et al.*, 2017). The disappearance of altered scoria in the samples collected in July 2000, and the increasing participation of glass shards, scoria and microcrystalline lithics is attributed to the rising of the magma to the surface and its progressive eruption through an open-vent system. In consequence, the onset of Phase I is related to the progressive cleaning of the vent due to rising of a renewed magma which was finally erupted since 2001 with an open-vent style (Fig. 8A and B). The low vesicularity and blocky shape of the juvenile fragments has been suggested by Cioni *et al.* (2014) as consequence of the shuttering of syn-eruptively degassed, crystallized, more rigid and volatile-rich magmas explosively fragmented, as it was observed during the 2010 Eyjafjallajökull eruption.

Further tephra emissions in 2002 and 2003 were produced by Strombolian and Vulcanian-like eruptions consisted of two varieties of juvenile scoria (black and brown) accompanied by higher amounts of glass shards (10-15%) which is consistent with an open vent system. The two different types of scoria ejected may be attributed to textural variations (such as crystallinity/vesicularity) or to the eruption of an heterogeneous melt (*i.e.,* magma mingling or an stratified magma column). However, the bulk ash geochemistry of these samples was quite stable (57.9-60.2 wt% SiO_2), similarly to the mineral phases identified via XRD (Table 5). This geochemical and mineralogical stability may be explained by the eruption of juvenile particles with different vesicularity and groundmass crystal content, which may suggest the fragmentation of a vertically heterogeneous magma column (Cioni *et al.,* 2014), or as result of varying magma supply rates as demonstrated by Wright *et al.*, (2012) within this period (Fig. 8B). From textural observations, can be suggested that both rheology and magma supply rates favor this juvenile textural bimodalities.

5.1.2. Phase II

The largest eruptions during 2006 showed long-lasting unrest periods in the months prior to the eruption (*e.g.,* Champenois *et al.,* 2014). There occurred a progressive decrease of black scoria in time, whereas the brown scoria increased. As previously suggested, these bimodal juvenile particles may be correlated to the stratification of the magma column in the conduit. This agrees with the increasing vesicularity of juvenile grains between April and August 2006, which suggest the progressive eruption of a volatile-saturated magma. In fact, for a given viscosity, increasing density of bubbles correlates with higher bubble nucleation rates that have been attributed to progressively later onset of bubble nucleation at higher degrees of supersaturation with volatiles (Houghton and Carey, 2015). Thus, the predominance of highly vesicular fragments suggests a prominent and active role of degassing-related magmatic fragmentation during the eruption (Cioni *et al.*, 2014). An additional fact is the shape of these vesicles. Elongated and fibrous vesicles, such as these observed in the 24 August samples are indicative of magma fragmentation due to a rapid acceleration of the system (Cashman *et al.,* 2000) or as representative of the central part of a magmatic column at the conduit during Plinian-type eruptions, where vesicles are free to grow only subjected to elongational stresses (Polacci, 2005). All these observations are coherent with the direct observations of the volcanic activity during 2006, which produced a stratospheric column (Fig. 8C). However, in contrast to the geochemical data obtained from samples collected from the rest of the time series, the bulk rock geochemistry at August 2006 reveals a silica-rich andesitic composition (62.3 wt% SiO_2). Additional changes are noticed from mineralogy by the first recognizance of akermanite and magnetite, higher amounts of plagioclase (>60%) and lower amounts of pyroxene (32-33%) together permanent olivine, all of them recognized via XRD as characteristic for this period. Thus, the compositional heterogeneity should indicate mixing of two magmas (Fig. 8C). This is in agreement with the observations made by several authors (*e.g.,* Fee *et al.,* 2010; Steffke *et al.,* 2010; Samaniego *et al.,* 2011; Eychenne *et al.,* 2013; Myers *et al.,* 2014). In fact, melt inclusion composition paired with host phenocryst zonation made by Myers *et al.* (2014) indicated mixing of two distinct magmas: a volatile-rich (~4.0 wt% H_2O and ~1,800 ppm S) basaltic andesite containing olivine phenocrysts and a degassed (~1.0 wt% H_2O and 100-500 ppm S) andesite with plagioclase and pyroxene phenocrysts that contain andesitic to dacitic melt inclusions.

5.1.3. Phase III

During the initial stage of Phase III in 2007, there was a new increase of hydrothermally altered reddish scoria and lithics (total amount 40-65%),

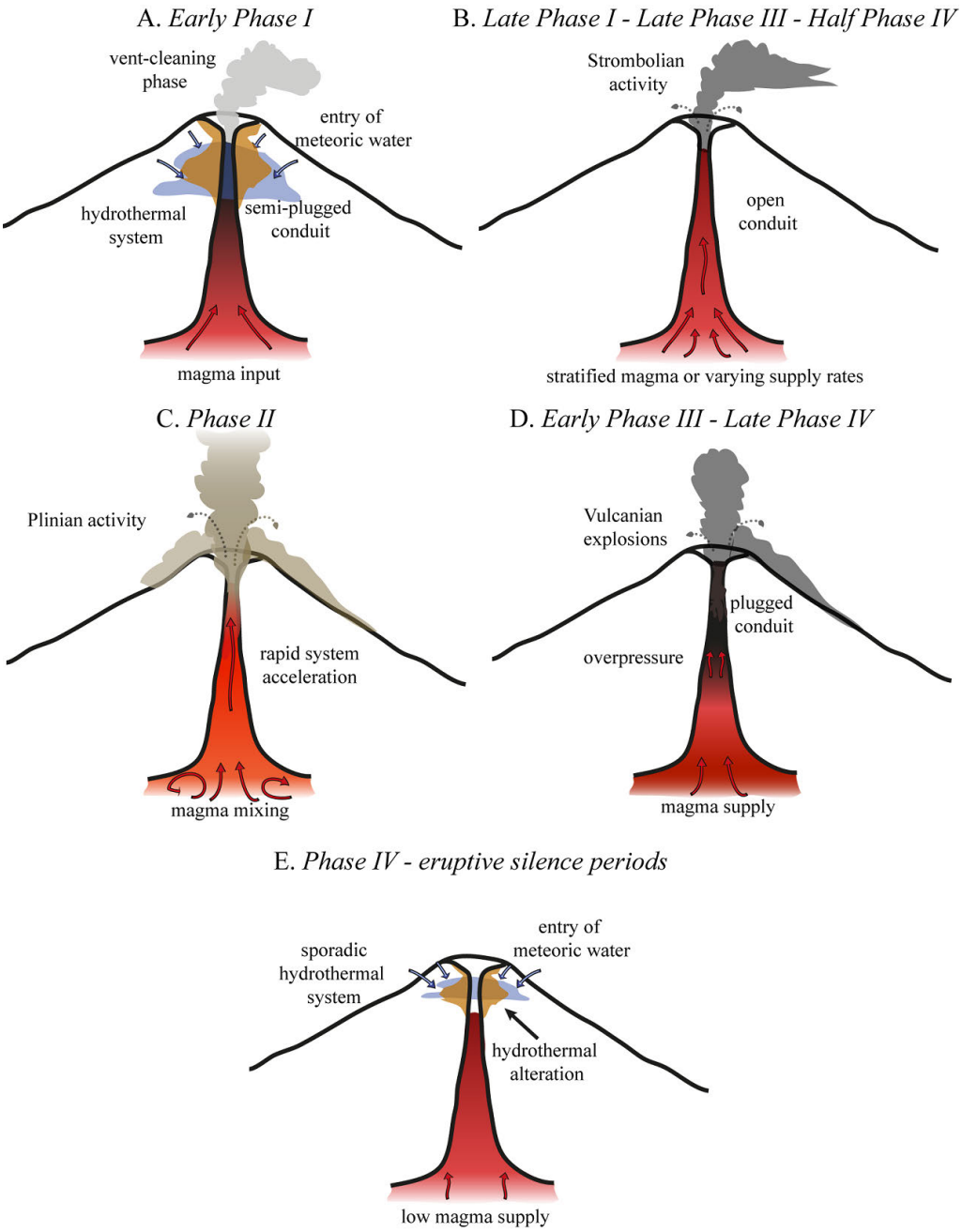

FIG. 8. Cartoons of the different eruption mechanisms operating in Tungurahua volcano between 1999 and 2013. **A.** Model of the early Phase I with the development of an initial phreatic eruption. Rising magma transfers heat to the hydrothermal system producing the eruption of recycled rocks, including hydrothermally altered wall rocks; **B.** Open conduit dynamics as observed in late phase I, late Phase III and partially in Phase IV. Varying magma supply rates or stratified conduit determines the transition between brittle and ductile fragmentation, producing juvenile particles with varying degree of vesicularity and variable shape; **C.** Magma mixing produces a volatile-saturated melt which triggers Plinian activity during Phase II; **D.** A decrease of magma supply rates may contribute to the plugging of the conduit and the over-pressurization of the magma column to trigger Vulcanian eruptions as in early Phase III and late Phase IV; **E.** Similarly to A, during eruptive silence periods in Phase IV the entry of meteoric water favored the formation of an sporadic hydrothermal system and local wall-rock hydrothermal alteration. Low magma supply was not able to trigger eruptions.

reaching similar proportions to juvenile particles (black scoria, free crystals and glass shards). There are not textural indicators of phreatomagmatic interactions in juvenile particles (there were only observed particles with blocky and fluid shapes), however the hydrothermal alteration, the amount of recycled material and the existence of fresh juvenile particles suggest a Vulcanian mechanism (Fig. 8D). For comparison, during the 1st February 2014 Tungurahua eruption, an average of 49.34% corresponded to non-juvenile material in tephra (38.16% lithics and 11.18% altered scoria), thus a minimum limit of 40% of recycled material will be here considered as indicative of Vulcanian eruptions.

Several fluid, filamentous and blocky shaped glassy particles were identified within the ashes of 5-6 February 2008. Melt droplets, preserved as fluidal clasts (filaments) are correlated to magmas that fragment in a hot fluid state (Houghton and Carey, 2015). These particles are most typically associated with small subaerial explosive eruptions of low-viscosity (<10^2 Pa s) basaltic melts, due to the deformation of low-viscosity lava in the air (Moune *et al.,* 2007). Thus, we can associate these particles to the alternation between ductile and brittle fragmentation of a hot magma, as result of varying rheology and/or sypply rate of the magma, similarly to Phase I. This agrees with the direct observation of alternating episodes of jetting and explosions (Biggs *et al.,* 2010).

The short-to medium-lived eruptions occurred since 2008, which erupted exclusively blocky juvenile material with low-to-moderate vesicularities is typical from Strombolian eruptions, and reflects the brittle fragmentation of volatile loaded magma (Fig. 8B).

5.1.4. Phase IV

Hydrothermally altered fragments, represented by reddish scoria was frequent in most of the samples since 2010 up to 2012, but always at lower amount than 30%, much lower than in Phase III. These tephras enriched in altered fragments were interspersed with some infrequent, purely juvenile tephras and a particular tephra fall full of lithics in December 27th 2011. At surface level, Vulcanian eruptions with little geophysical warning are inferred from eyewitness observations within this period and also in the following years (*e.g.,* Hall *et al.,* 2015; Mothes *et al.,* 2015; Parra *et al.,* 2015; Kim *et al.,* 2014; Romero *et al.*, 2017). However, Vulcanian events are characterized by a series of physical properties and distinguishable eruptive products (*e.g.,* Clarke *et al.,* 2015; Morrisey and Mastin, 2000) such as >40% of recycled particles within tephra, as we previously established for Tungurahua (Phase III and 1st February 2014) which was not observed between 2010 and 2012, with the only exception of the December 2012 event. In addition, vesicularity of juvenile particles was zero or moderate-to-high, not spanning a wide range as frequently observed during Vulcanian eruptions (*e.g.,* Clarke *et al.,* 2015). These particles also exhibited ductile fragmentation features such as fluid and filamentous shapes, despite fewer blocky shapes were observed. Pure magmatic dynamics, especially during Strombolian activity is more prone to produce these particles (Fig. 8B). This is also supported by the eruption of dominant pumice in 2013. Thus, at this point the origin of hydrothermally altered grains remains unclear. Then, was Tungurahua able to develop an active hydrothermal system (necessary condition to provide hydrothermally altered particles) during the paucity of magmatic eruptions?. Even when the heat transfer from shallow magma batches is not favorable for the existence of an hydrothermal system, the development of a reduced or sporadic hydrothermal system is possible, as indicated by geochemical and isotopic characterization of springs and bubbling waters sampled at Tungurahua, which are Cl-SO_4 earth-alkaline, medium salinity and significant He-mantle signature (around 60%) fluids (Inguaggiato *et al.*, 2010). Thus, the lesser amounts of hydrothermally altered particles between 2010 and 2013 are likely related to a harder involvement of water in the system during the non-eruptive stages, and not to conduit plugging. This condition was favored by the episodic frequency of eruptions, which permitted the infiltration of meteoric water into the conduit (Fig. 8E). Even more, the episodic frequency of these eruptions was probably not associated to the conduit plugging, but yet correlated to a change in the magma supply rate or an increase in the viscosity of magma intrusions. This is well constrained with the geochemical variations observed in the year 2012-2013 which may be interpreted as the intrusion of a "renewed" (deeper, volatile-rich magma) triggering magma mixing and eruption, as it is also noticed by Myers *et al*. (2014) in 2010. Even though a single Vulcanian eruption is identified using tephra between 2010 and 2013, further eruptions at the end of

Phase IV (2013-2014) were well recognized as Vulcanian (*e.g.,* Hall *et al.,* 2015; Parra *et al.,* 2015; Romero *et al.*, 2017). The transition in time from open to a plugged conduit suggest a progressive decrease of the magmatic ascent rates or the increase in magma viscosity through time.

5.2. Magmatic processes feeding eruptive transitions

Within its geological and historical eruptive history, Tungurahua products range from basaltic andesites to dacites, with subordinate rhyolites, and a typical plg + cpx + opx ± hbl ± ol ± Fe-Ti oxides mineral assemblage (Hall *et al.,* 1999; Bustillos, 2008; Samaniego *et al.,* 2011). The rock compositions from ancient and modern Tungurahua edifices (I, II and III) (Hall *et al.,* 1999; Bustillos *et al.,* 2011) turn out to be similar to the composition of tephra emitted between 1999 and 2013, as they are both medium- to high-K andesites (54-58 wt% SiO_2). If we assume that analytical issues are avoided during the sampling and analytical processes, the absence of linear trends in variation diagrams and the separation between the 2012-2013 and the rest of the samples may be related to different temperature, pressure and/or water content conditions at the source of these magmas and reject a differentiation or fractionation process from a similar magmatic source. This could be complementary to that proposed by Myers *et al.* (2014) on the co-existance of several magma reservoirs at different depth (shallow, 1-3 km under the base of the volcano and a deep reservoir at >7 km depth).

5.3. Tephra GSD

5.3.1. Depositional processes inferred

According to Eychenne *et al.* (2012), the eruption of August 2006 at Tungurahua had bimodal GSD deposits controlled by two synchronous processes: lapilli deposition from the main plume and fine ash elutriated from PDCs. This situation was also shown by Bernard *et al.* (2016). At least 5 eruptive phases produced PDCs from 2007 to 2013 (March 2007, February 2008, May and December 2010, December 2012, May and July 2013) (Hall *et al.,* 2015; Bustillos *et al.,* 2016), which is in good agreement with the increase of bimodal and trimodal GSDs from 2009 to 2013. For example, the major eruption occurred in May 28th 2010, which produced an eruption column of 10 km above the crater level (a.c.l.) and a series of PDCs, corresponds to deposits with bimodal GSD characterized by two opposite modes at fine lapilli (-0.74Φ) and very fine ash (4.23Φ) (Table 3). These features are not unique for purely-magmatic, large scale eruptions, as they are also observed in moderate Vulcanian eruptions occurred later in 2013 and 2014 (*e.g.,* Parra *et al.,* 2015; Romero *et al.,* 2017).

Particle aggregation has been also associated with bimodal or polymodal GSDs in the literature (*e.g.,* Scasso *et al.,* 1994; Durant *et al.,* 2009). We suggest that trimodal GSD in sample 18B is related to particle aggregation, as evidenced by the SEM analyses which show abundant aggregates that correspond to coated particles, bound by hydro-bonds and electrostatic forces, and in most cases are poorly preserved due to the particle impact during fall (particle type PC2 in Brown *et al.,* 2012). As Tungurahua area annually receives a notable amount of rainfall (about 3000 mm; Jones *et al.*, 2015) we suspect that the humidity provided by these atmospheric processes could favor the formation of aggregates during explosive eruptions, especially when no phreatic eruptive mechanism is suspected through ash analyses. Although thunderstorms/lightning are not often reported in this area (*e.g.,* Rollenbeck and Bendix, 2011) but they may occasionally promote the formation of aggregates. Nevertheless, these two explanations do not account for all the bimodal and trimodal deposits and should be considered as alternative mechanisms of ash aggregation in this area.

In the case of samples not generated during PDC-forming eruptions or ash aggregation, a third deposition mechanism is required. Possible explanations are: **1)** the nature of Vulcanian events that may erupt both fine and coarse grained tephra including ballistic rocks (*e.g.,* Fierstein *et al.,* 1997; Cashman *et al.,* 2000; Houghton *et al.,* 2004; Clarke *et al.,* 2015), which may be deposited together, especially in the proximal zones as our sampling stations; or **2)** the plume dispersal patterns, including plume bifurcation, wind direction variability and deposition of long-lasting (tens of days) eruptions that produce millimeter-thick deposits with complex dispersals and non-elliptic isopachs (Bernard *et al.,* 2013). This would generate modes with different, but not extreme grain sizes (*i.e.,* very fine grained or very coarse grained), as seen in table 3 for all the samples prior to 2006.

We suggest that, during the first 7 years of eruptions (1999-2006), processes like plume bifurcation and

sedimentation of multiple plumes were responsible of most polymodal GSD (Fig. 9A), while during and after 2006 there was a combination of deposition processes that generated bimodal/ trimodal GSD deposits, such as interaction between plume and co-PDC deposition (Fig. 9B), Vulcanian fragmentation (Fig. 9B), and the variability of tephra plumes. As an accessory and marginal process, we suggest that ash aggregation could be produced during strong thunders or lighting in the area of Tungurahua (Fig. 9C).

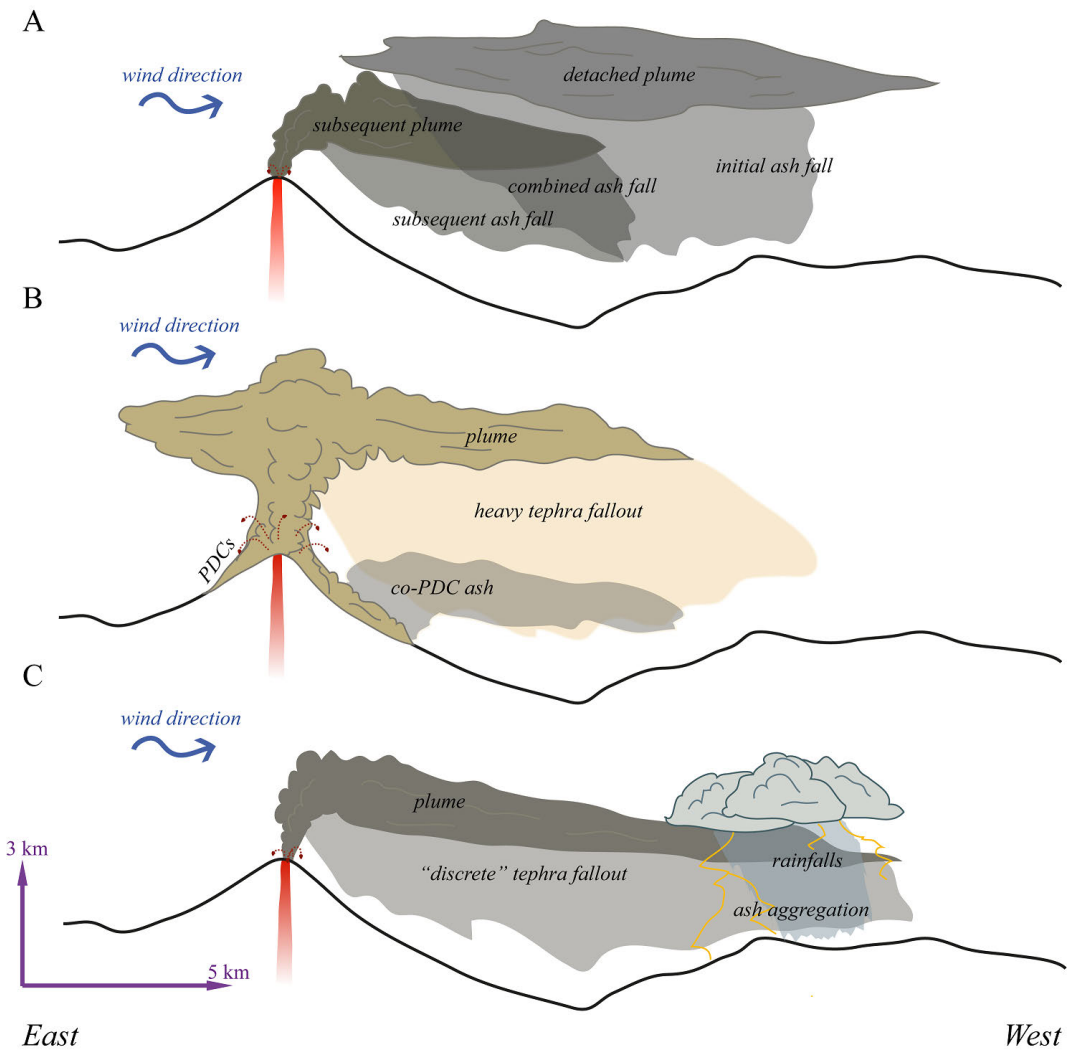

FIG. 9. Cartoons of the different fall out mechanisms proposed for tephra fall deposits at Tungurahua volcano. **A.** When no major eruptions or atmospheric anomalies are occurring, transitions in eruptive style (*e.g.,* phreatic to Strombolian, Vulcanian to Strombolian or similar cases), produce variations in the dispersal pattern of tephra and spasmodic activity produce tephra deposits with polymodal GSD; **B.** Major eruptions (purely magmatic as in August 2006 or Vulcanian-triggered as in 28 May 2010 or 14 July 2013, VEI ~3) may develop high eruptive columns (>10 km; not to scale in figure) with "heavy" tephra fall, including lapilli-to bomb-sized fragments at ~10 km radius from the vent, together with abundant ash. Pyroclastic density currents (PDCs) flowing down the flanks of the volcano might contribute fine material associated with co-PDC clouds. This was shown by Bernard *et al.* (2016) for the August 2006 eruption. Ballistics at a distance up to 4-5 km are common. The combination of all of those products may be responsible of polymodal GSD in tephra samples; **C.** During "weak" eruptions (VEI 1-2) atmospheric anomalies (*i.e.,* rain fall and/or electrical storms) may induce particle coating leading to the formation of ash aggregates. In areas without these disruptions, tephra fall will probably produce unimodal or bimodal grain size distribution.

5.3.2. Potential health impacts

Acute respiratory manifestations seen after heavy ash falls include irritation of the chest, nose and throat discomfort, but also acute exacerbations of asthma and bronchitis are seen (Gudmundsson, 2011). As shown in table 3, the extremely fine ash particle size, both thoracic and *respirable* (breathable) (<10 and <4 μm, respectively) have been calculated using the method of Horwell and Baxter (2006). The average proportion of Tungurahua's *respirable*-sized ash is estimated at ~5 wt% (range from 0.07 to 13.64 wt%) nevertheless no crystalline silica (*i.e.,* quartz, cristobalite or tridimite) has been identified via XRD. In addition, filamentous glassy particles (known for being abrasive; *e.g.,* Horwell and Baxter, 2006) are always observed in larger sizes (>200 μm) than for respirable or alveolar particles. Thus, the ash of Tungurahua has to be considered as potentially harmful for human health as a result of long-lasting exposure, especially because it may trigger acute health problems despite chronic diseases. This is in agreement with direct health observations, as epidemiological map has changed in the villages affected by the volcano while bronchial asthma, cough, throat irritation, eye irritation and respiratory allergies, and altered pulmonary capacity (spirometry) has been reported after Tungurahua ash exposure (Paladines and Zamora, 2011; Cifuentes and Alvarado, 2015)

6. Conclusions

Some conclusions derived from our research are listed below:

a. During the initial stage (1999-2000) of the current eruptive cycle at Tungurahua, a progressive conduit cleaning is observed as the eruption elapses. At the beginning of the eruption in 1999 phreatic mechanism has been interpreted, as no evidence of phreatomagmatic activity has been found using the current methods. The ashes then erupted in 2001 revealed the explosive fragmentation of a degassed, crystallized and "rigid" magma. In contrast, the juvenile products erupted after in 2002 and 2003 exhibited bimodal textures and compositional (chemistry and mineralogy) homogeneity, and we suggest they reflect variations in both magma supply rate and its rheology within a stratified magma column, without any evidence of the interaction between two different magma intrusions.
b. The progressive variation of the 2006 Plinian eruption and associated tephra components, in addition to the textural changes observed in juvenile particles suggest that these eruptions were fed by a volatile-saturated magma, thus the fragmentation of magma occurred by its degassing and its rapid acceleration within the conduit. Even more, the evidence from geochemistry and mineral phases indicate a compositional change of the magma if compared to the pre-2006 series, which is in agreement with the previously reported mixing of two magmas (*e.g.,* Samaniego *et al.,* 2011; Myers *et al.*, 2014).
c. During early 2007, the eruption of high amounts recycled particles (40-65%) accompanied by juvenile particles are compatible with a series of Vulcanian eruptions. In contrast, the eruptions then occurred in 2008 were magmatic and ejected both fluid and brittle-fragmented juveniles during jetting periods and explosions. This is interpreted as a result of varying rheology and/or supply rate of the magma, similarly as seen in 2002-2003. The short-to medium-lived eruptions occurred since 2008, ejected blocky juveniles as typically seen during Strombolian eruptions, and reflects the brittle fragmentation of volatile loaded magma.
d. Varying amounts of hydrothermally altered particles (always <30%) between 2010-2013 are likely related to a harder involvement of water in the system during the periods of eruptive silence, which certainly permitted the infiltration of meteoric water into the conduit. The textural features of juvenile particles suggest a dominant ductile fragmentation associated to Strombolian activity. Formal Vulcanian events are newly recognized in December 2011 and widely observed since 2013. The transition in time from open to plugged conduit dynamics suggest a progressive decrease of the magmatic ascent rates or the increase in magma viscosity through time.
e. From grain size analyses, we propose two first order phenomena during tephra deposition: **1)** plume bifurcation and sedimentation of multiple plumes were responsible of most polymodal GSD, mainly occurring between 1999 and 2006; **2)** deposits with bimodal/trimodal GSD as consequence of interaction between plume and co-PDC deposition (PDC elutriation), Vulcanian fragmentation, and the variability of tephra plumes during and after 2006; a second order factor could be ash

aggregation during strong thunders or lighting in the area of Tungurahua.

f. Due to its mechanical properties, the ash of Tungurahua has to be considered as potentially harmful for human health as a result of long-lasting exposure, especially because it may trigger acute health problems despite chronic diseases. Not crystalline silica has been identified.

g. This study demonstrates that periodic and systematic tephra fall sampling at long-lasting erupting volcanoes is a valuable tool for understanding the eruptive mechanisms and the processes and impacts related to tephra falls, especially at inhabited areas.

Acknowledgements

This project contains partial results from the Ph.D. thesis of A. Guevara. Laboratory (XRF, XRD and SEM-EDS) analyses were supported by the DEMEX (Departamento de Metalurgia Extractiva) from Escuela Politécnica Nacional. We thank the fruitful comments of Dr. H. Delgado Granados (Universidad Autónoma de México) and Dr. F. Maeno (University of Tokio), plus the English review given by translator P. Soto. We acknowledge to the reviewers, Drs. H. Moreno Roa and D. Sellés by their very helpful comments which certainly improved this manuscript. Also, the editorial handling of Dr. W. Vivallo was essential.

References

Almeida, E.; Ramón, P. 1991. Las erupciones históricas del volcán Tungurahua. Boletín Geológico Ecuatoriano 2: 89-138.

Arellano, S.R.; Hall, M.; Samaniego, P.; Le Pennec, J-L.; Ruiz, A.; Molina, I.; Yepes, H. 2008. Degassing patterns of Tungurahua volcano (Ecuador) during the 1999-2006 eruptive period, inferred from remote spectroscopic measurements of SO_2 emissions. Journal of Volcanology and Geothermal Research 176 (1): 151-162.

Aspden, J.; Jemielita, R.; Litherland, M.; Bermúdez, R.; Bolaños, J.; Pozo, M.; Viteri, F.; Celleri, M. 1994. Geological and Metal Occurrence maps of the Northern Cordillera Real, Metamorphic Belts, Ecuador. British Geological Survey 11. 1:500.000.

Bernard, B.; Bustillos, J.; Wade, B.; Hidalgo, S. 2013. Influence of the wind direction variability on the quantification of tephra fallouts: December 2012 and March 2013 Tungurahua eruptions. Avances en Ciencias e Ingenierías 5 (1): A14-A21.

Bernard, J.; Eychenne, J.; Le Pennec, J. L.; Narváez, D. 2016. Mass budget partitioning during explosive eruptions: insights from the 2006 paroxysm of Tungurahua volcano, Ecuador. Geochemistry, Geophysics, Geosystems 17 (8): 3224-3240.

Biggs, J.; Mothes, P.; Ruiz, M.; Amelung, F.; Dixon, T.H.; Baker, S.; Hong, S.-H. 2010. Stratovolcano growth by co-eruptive intrusion: The 2008 eruption of Tungurahua Ecuador. Geophysical Research Letters 37: L21302.

Blott, S.J.; Pye, K. 2001. Gradisat: A grain size distribution and statistics package for the analysis of unconsolidated sediments. Earth Surface Processes and Landforms 26: 1237-1248.

Bonadonna, C.; Macedonio, G.; Sparks, R.S.J. 2002. Numerical modeling of tephra fallout associated with dome collapse and Vulcanian explosions: application to Hazard assessment on Monserrat. *In* The eruption of Soufriere Hills Volcano, from 1995 to 1999 (Druitt, T. H.; Kokelaar , B.P.; editors). Geological Society, London, Memoirs 21: 517-537.

Brown, R.J.; Bonadonna, C.; Durant, A.J. 2012. A review of volcanic ash aggregation. Physics and Chemistry of the Earth 45-46: 65-78.

Büttner, R.; Dellino, P.; Zimanowski, B. 1999. Identifying magma-water interaction from the surface features of ash particles. Nature 401 (6754): 688 p.

Bustillos, J. 2008. Las Avalanchas de Escombros en el sector del volcán Tungurahua. Tesis de Grado (Inédito). Escuela Politécnica Nacional: 151 p.

Bustillos, J. 2010. Transición del estilo eruptivo durante las erupciones andesíticas en sistema abierto: Contribución al estudio de los depósitos de ceniza del volcán Tungurahua. Master Thesis (Inédito), Nice Sophia Antipolis University: 48 p. France.

Bustillos, J.; Mothes, P. 2010. Ash falls at Tungurahua volcano: implementation of systematic ash collection for quantifying accumulated volumes. Cities On Volcanoes, No. 6, abstract volume: 2.7-O-07. Tenerife, Canary Island, Spain.

Bustillos, J.; Ruiz, G.; Le Pennec, J. 2011. Volcán Tungurahua: Cálculo indirecto del material sólido emitido. *In* Jornadas en Ciencias de la Tierra, No. 7, Equator Meetings S.A., ISBN: 978-9978-383-17-9. Quito.

Bustillos, J.; Guevara, A.; Hidalgo, S. 2013. Los depósitos de ceniza del 04 y 05 de Mayo 2013 en el volcán Tungurahua. Pyroclastic Flow 3 (1): 1-8.

Bustillos, J.; Romero, J.; Troncoso, L.; Guevara, A. 2016. Tephra fall at Tungurahua Volcano (Ecuador)-1999-2014: An example of tephra accumulation from a long-lasting eruptive cycle. Geofísica Internacional 55 (1): 363-386.

Cannata, C.B.; De Rosa, R.; Donato, P.; Taddeucci, J. 2014. Ash Features from Ordinary Activity at Stromboli Volcano. International Journal of Geosciences 5: 1361-1382.

Carey, S.; Sigurdsson, H. 1982. Influence of particle aggregation on deposition of distal tephra from the May 18, 1980 eruption of Mount St. Helens volcano. Journal of Geophysical Research 87: 7061-7072.

Cas, R.A.F.; Wright, J.V. 1987. Volcanic successions: Modern and ancient: a geological approach to processes. Allen and Union: 528 p. London.

Cashman, K.V.; Sturtevant, B.; Papale, P.; Navon. 2000. Magmatic Fragmentation. *In* Encyclopedia of Volcanoes (Sigurdsson, H.; Houghton, B.; Rymer, H.; Stix, J.; McNutt, S.; editors). Academic Press: 1417 p.

Castro, A. 2013. Tonalite-granodiorite suites as cotectic systems: a review of experimental studies with application to granitoid petrogenesis. Earth-Science Reviews 124: 68-95.

Champenois, J.; Pinel, V.; Baize, S.; Audin, L.; Jomard, H.; Hooper, A.; Alvarado, A.; Yepes, H. 2014. Large-scale inflation of Tungurahua volcano (Ecuador) revealed by Persistent Scatterers SAR interferometry. Geophysical Research Letters 41 (16): 5821-5828.

Cifuentes, A.C.; Alvarado, L.A. 2015. Efecto en la salud respiratoria de las comunidades de Pillate, Manzano y Chonglontus expuestas crónicamente a la inhalación de ceniza del volcán Tungurahua. Tesis (Inédito). Universidad de las Américas: 47 p.

Cioni, R.; D'Oriano, C.; Bertagnini, A. 2008. Fingerprinting ash deposits of small scale eruptions by their physical and textural features. Journal of Volcanology and Geothermal Research 177 (1): 277-287.

Cioni, R.; Pistolesi, M.; Bertagnini, A.; Bonadonna, C.; Hoskuldsson, A.; Scateni, B. 2014. Insights into the dynamics and evolution of the 2010 Eyjafjallajökull summit eruption (Iceland) provided by volcanic ash textures. Earth and Planetary Science Letters 394: 111-123.

Clarke, A.B.; Ongaro, T.E.; Belousov, A.; 2015. Vulcanian eruptions. *In* The Encyclopedia of Volcanoes (Sigurdsson, H.; Houghton, B.; McNutt, S.; Rymer, H.; Stix, J.; editors). Elsevier: 1456 p.

Dellino, P.; Kyriakopoulos, K. 2003. Phreatomagmatic ash from the ongoing eruption of Etna reaching the Greek island of Cefalonia. Journal of Volcanology and Geothermal Research 126: 341-345.

Dellino, P.; La Volpe, L. 1995. Fragmentation versus transportation mechanisms in the pyroclastic sequence of Monte Pilato-Rocche Rosse (Lipari, Italy). Journal of Volcanology and Geothermal Research 64: 211-232.

Díaz-Alvarado, J.; Castro, A.; Fernández, C.; Moreno-Ventas, I. 2011. Assessing bulk assimilation in cordierite-bearing granitoids from the Central System batholith, Spain; experimental, geochemical and geochronological constraints. Journal of Petrology 52, 223-256.

Douillet, G.A.; Pacheco, D.A.; Kueppers, U.; Letort, J.; Tsang-Hin-Sun, È.; Bustillos, J.; Hall, M.; Ramón, P.; Dingwell, D.B. 2013a. Dune bedforms produced by dilute pyroclastic density currents from the August 2006 eruption of Tungurahua volcano, Ecuador. Bulletin of Volcanology 75: 762 p. doi:10.1007/s00445-013-0762-x.

Douillet, G.A.; Tsang-Hin-Sun, E.; Kueppers, U.; Letort, J.; Pacheco, D.A.; Goldstein, F.; Von Aulock, F.; Lavallée, Y.; Hanson, J.B.; Bustillos, J.; Robin, C.; Ramón, P.; Hall, M.; Dingwel, D.B. 2013b. Sedimentology and geomorphology of the deposits from the August 2006 pyroclastic density currents at Tungurahua volcano, Ecuador. Bulletin of Volcanology 75: 765 p. doi: 10.1007/s00445-013-0765-7.

Durant, A.J.; Rose, W.I.; Sarna-Wojcicki, A.M.; Carey, S.; Volentik, A.C.M. 2009. Hydrometeor-enhanced tephra sedimentation: constraints from the 18 May, 1980 eruption of Mount St. Helens. Journal of Geophysical Research 114: B03204.

Eychenne, J.; Le Pennec, J-L.; Troncoso, L.; Gouhier, M.; Nedelec, J.M. 2012. Causes and consequences of bimodal grain-size distribution of tephra fall deposited during the August 2006 Tungurahua eruption (Ecuador). Bulletin of Volcanology 74: 187-205.

Eychenne, J.; Le Pennec, J-L.; Ramón, P.; Yepes, H. 2013. Dynamics of explosive paroxysms at open-vent andesitic systems: High resolution mass distribution analyses of the 2006 Tungurahua fall deposit (Ecuador). Earth and Planetary Science Letters 361: 343-355.

Fee, D.; Garcés, M.; Steffke, A. 2010. Infrasound from Tungurahua Volcano 2006-2008: Strombolian to Plinian activity. Journal of Volcanology and Geothermal Research 193: 67-81.

Fierstein, J.; Houghton, B.F.; Wilson, C.J.N.; Hildreth, W. 1997. Complexities of plinian fall deposition at vent: an example from the 1912 Novarupta eruption(Alaska). Journal of Volcanology and Geothermal Research 76: 215-227.

Folk, R.L.; Ward, W.C. 1957. Brazos river bar: A study in the significance of grain size parameters. Journal of Sedimentary Petrology 27: 3-26.

Gaunt, H.E.; Bernard, B.; Hidalgo, S.; Proaño, A.; Wright, H.; Mothes, P.; Criollo, E.; Kueppers, U. 2016. Juvenile

magma recognition and eruptive dynamics inferred from the analysis of ash time series: The 2015 reawakening of Cotopaxi volcano. Journal of Volcanology and Geothermal Research 328: 134-146.

Goodyear, J.; Duffin, W.J. 1954. The identification and determination of plagioclase feldspars by the X-ray powder method. Mineralogical Magazine 30: 306-326.

Gudmundsson, G. 2011. Respiratory health effects of volcanic ash with special reference to Iceland. A review. The Clinical Respiratory Journal 5 (1): 2-9.

Hall, M.; Robin, C.; Beate, B.; Mothes, P.; Monzier, M. 1999. Tungurahua Volcan, Ecuador: structure eruptive history and hazards. Journal of Volcanology and Geothermal Research 91: 1-21.

Hall, M.L.; Samaniego, P.; Le Pennec, J-L.; Johnson, J.B. 2008. Ecuadorian Andes volcanism: A review of Late Pliocene to present activity. Journal of Volcanology and Geothermal Research 176 (1): 1-6.

Hall, M.; Steele, A.L.; Mothes, P.A.; Ruiz, M.C. 2013. Pyroclastic density currents (PDC) of the 16-17 August 2006 eruptions of Tungurahua volcano, Ecuador: Geophysical registry and characteristics. Journal of Volcanology and Geothermal Research 265: 78-93.

Hall, M.L.; Steele, A.; Bernard, B.; Mothes, P.; Vallejo, S.; Doulliet, G.A.; Ramón, P.; Aguaiza, S.; Ruiz, M. 2015. Sequential plug formation, desintegration by vulcanian explosions, and the generation of granular pyroclastic density currents at Tungurahua volcano (2013-2014), Ecuador. Journal of Volcanology and Geothermal Research 306: 90-103. doi: 10.1016/j.jvolgeores.2015.09.009.

Heiken, G.; Wohletz, K.H. 1985. Volcanic Ash. University of California Press: 245 p. Berkeley.

Hidalgo, S.; Battaglia, J.; Arellano, S.; Steele, A.; Bernard, B.; Bourquin, J.; Galle, B.; Arrais, S.; Vásconez, F. 2015. SO_2 degassing at Tungurahua volcano (Ecuador) between 2007 and 2013: transition from continuous to episodic activity. Journal of Volcanology and Geothermal Research 298: 1-14.

Horwell, C.J.; Baxter, P.J. 2006. The respiratory health hazards of volcanic ash: a review for volcanic risk mitigation. Bulletin of Volcanology 69 (1): 1-24. doi: 10.1007/s00445-006-0052-y.

Houghton, B.F.; Carey, R.J. 2015. Pyroclastic Fall Deposits. *In* The Encyclopedia of Volcanoes (Sigurdsson, H.; Houghton, B.; McNutt, S.; Rymer, H.; Stix, J.; editors). Elsevier: 1456 p.

Houghton, B.F.; Smith, R.T. 1993. Recycling of magmatic clasts during explosive eruptions: estimating the true juvenile content of phreatomagmatic volcanic deposits. Bulletin of Volcanology 55 (6): 414-420.

Houghton, B.F.; Wilson, C.J.N.; Fierstein, J.; Hildreth, W. 2004. Complex proximal deposition during the Plinian eruptions of 1912 at Novarupta, Alaska. Bulletin of Volcanology 66: 95-133.

Inguaggiato, S.; Hidalgo, S.; Beate, B.; Bourquin, J. 2010. Geochemical and isotopic characterization of volcanic and geothermal fluids discharged from the Ecuadorian volcanic arc. Geofluids 10 (4): 525-541.

Jones, R.; Manville, V.; Andrade, D. 2015. Probabilistic analysis of rain-triggered lahar initiation at Tungurahua volcano. Bulletin of Volcanology 77 (8): 68 p.

Kley, J.; Monaldi, C.; Salfity, J. 1999. Along-strike segmentation of the Andean foreland; causes and consequences. Tectonophysics 301: 75 -94.

Kim, K.; Lees, J. M.; Ruiz, M.C. 2014. Source mechanism of Vulcanian eruption at Tungurahua Volcano, Ecuador, derived from seismic moment tensor inversions. Journal of Geophysical Research: Solid Earth 119: 1145-1164.

Lautze, N.; Taddeucci, J.; Andronico, D.; Cannata, Ch.; Tornetta, L.; Scarlato, P.; Houghton, B.; Lo Castro, M. 2012. SEM-based methods for the analysis of basaltic ash from weak explosive activity at Etna in 2006 and the 2007 eruptive crisis at Stromboli. Physics and Chemistry of the Earth (A) 45-46: 113-127.

Le Maitre, R.W. 1984. A proposal by the IUGS Subcommission on the Systematics of Igneous Rocks for a chemical classification of volcanic rocks based on the total alkali silica (TAS) diagram: (on behalf of the IUGS Subcommission on the Systematics of Igneous Rocks). Australian Journal of Earth Sciences 31 (2): 243-255.

Le Pennec, J-L.; Mothes, P.; Ramón, P.; Ruiz, G. 2002. Maximum and minimum volume estimates of an ash fall layer from the august 2001 eruption of Mt Tungurahua (Ecuador). *In* International Society for Animal Genetics: ISAG, No. 5, Extended Abstract: 371-374. Toulouse, France.

Le Pennec, J.-L.; Ruiz, A.G.; Mothes, P.; Hall, M.; Alvarado, A.; García, A.; Segovia, M. 2004. Estimación del volumen del depósito de ceniza de la erupción de Agosto 2001 del Volcán Tungurahua: Investigaciones en Geociencias 1: 13-18.

Le Pennec, J-L.; Hall, M.; Robin, C.; Bartomioli, E. 2006. Tungurahua Volcano, Late Holocene Activity. Field Guide, Cities on Volcanoes, No. 4: 24 p. Quito.

Le Pennec, J-L.; Jaya, D.; Samaniego, P.; Ramón, P.; Moreno-Yánez, S.; Egred, J.; Van Der Plicht, J. 2008. The AD 1300-1700 eruptive periods at Tungurahua volcano,

Ecuador, revealed by historical narrative, stratigraphy and radiocarbon dating. Journal of Volcanology and Geothermal Research 176: 70-81.

Le Pennec, J.L.; Ruiz, G.A.; Ramón, P.; Palacios, E.; Mothes, P.; Yepes, H. 2012. Impact of tephra falls on Andean communities: the influences of eruption size and weather conditions during the 1999-2001 activity of Tungurahua volcano, Ecuador. Journal of Volcanology and Geothermal Research 217: 91-103.

Litherland, M.; Egüez, A. 1993. Mapa Geológico de la República del Ecuador 1:1,000,000. British Geological Survey (Keyworth, Nottingham) and CODIGEM, Quito, Ecuador.

Molina, I.; Kumagai, H.; Le Pennec, J-L.; Hall, M. 2005. Three-dimensional P-Wave velocity structure of Tungurahua volcano, Ecuador. Journal of Volcanology and Geothermal Research 147: 144-156.

Morrissey, M.; Mastin, L.G. 2000. Vulcanian eruptions. *In* Encyclopedia of Volcanoes (Sigurdsson, H.; Houghton, B.; Rymer, H.; Stix, J.; McNutt, S.; editors). Academic Press: 1417.

Mothes, P.; Yepes, H.A.; Hall, M.L.; Ramón, P.A.; Steele, A.L.; Ruiz, M. 2015. The scientific-community interface over the fifteen years eruptive episode of Tungurahua Volcano, Ecuador. Journal of Applied Volcanology 4: 9 p.

Moune, S.; Faure, F.; Gauthier, P.J.; Sims, K.W. 2007. Pele's hairs and tears: natural probe of volcanic plume. Journal of Volcanology and Geothermal Research 164 (4): 244-253.

Myers, M.L.; Geist, D.J.; Rowe, M.C.; Harpp, K.S.; Wallace, P.J.; Dufeck, J. 2014. Replenishment of volatile-rich mafic magma into a degassed chamber drives mixing and eruption of Tungurahua volcano. Bulletin of Volcanology 76: p. 872. doi: 10.1007/s00445-014-0872-0.

Paladines, J.L.; Zamora, C.P. 2011. Impacto provocado por el volcán Tungurahua en la salud de los pobladores de Penipe durante el período eruptivo comprendido entre el año 2003-2010. Tesis (Inédito). Pontificia Universidad Católica del Ecuador: 134 p.

Parra, R.; Bernard, B.; Narváez, D.; Le Pennec, J-L.; Hasselle, N.; Folch, A. 2015. Eruption Source Parameters for forecasting ash dispersion and deposition from vulcanian eruptions at Tungurahua volcano: Insights from field data from the July 2013 eruption.Journal of Volcanology and Geothermal Research 309: 1-13. doi: 10.1016/j.jvolgeores.2015.11.001.

Polacci, M. 2005. Constraining the dynamics of volcanic eruptions by characterization of pumice textures. Annals of Geophysics 48 (4-5): 731-738.

Rollenbeck, R.; Bendix, J. 2011. Rainfall distribution in the Andes of southern Ecuador derived from blending weather radar data and meteorological field observations. Atmospheric Research 99 (2): 277-289.

Romero, J.E.; Douillet, G.A.; Vargas, S.V.; Bustillos, J.; Troncoso, L.; Alvarado, J.D.; Ramón, P. 2017. Dynamics and style transition of a moderate, Vulcanian-driven eruption at Tungurahua (Ecuador) in February 2014: pyroclastic deposits and hazard considerations. Solid Earth 8 (3): 697 p.

Ruiz, G.; Barba D.; Yepes, H.; Hall, M. 2004. Las Nubes de Ceniza del Volcán Tungurahua entre Octubre de 1999 y Septiembre de 2001. Investigaciones en Geociencias, Instituto Geofísico, Escuela Politécnica Nacional 1: 28-34.

Ruiz, A.; Le Pennec, J.-L.; Palacios, E.; Hall, M.; Yepes, H. 2006. Indirect estimation of ash fall volume deposited near Tungurahua volcano (Ecuador) from Oct. 1999 to Dec. 2004. Cities on Volcanoes IAVCEI, No. 4: p. 27. Quito.

Samaniego, P.; LePennec, J-L.; Robin, C.; Hidaldo, S. 2011. Petrological analysis of the pre-eruptive magmatic process prior to the 2006 explosive eruptions at Tungurahua volcano (Ecuador). Journal of Volcanology and Geothermal Research 199: 69-84.

Scasso, R.A.; Corbella, H.; Tiberi, P. 1994. Sedimentological analysis of the tephra from the 12-15 August 1991 eruption of Hudson volcano. Bulletin of Volcanology 56: 121-132.

Sheridan, M.F.; Marshall, J.R. 1983. Interpretation of Pyroclast Surface Features Using SEM Images. Journal of Volcanology and Geothermal Research 16: 153-159.

Steffke, A.; Fee, D.; Garces, M.; Harris, A. 2010. Eruption chronologies, plume heights and eruption styles at Tungurahua volcano: Integrating remote sensing techniques and infrasound. Journal of Volcanology and Geothermal Research 193: 143-160.

Stern, C.R. 2004. Active Andean volcanism: its geologic and tectonic setting. Revista Geológica de Chile 31 (2): 161-206. doi: 10.5027/andgeoV31n2-a01.

Stone, J.; Barclay, J.; Simmons, P.; De Cole, P.; Loughlin, S.; Ramón, P.; Mothes, P. 2014. Risk reduction through community-based monitoring: the vigías of Tungurahua, Ecuador. Journal of Applied Volcanology 3: 11 p.

Taddeucci, J.; Edmonds, M.; Houghton, B.; James, M.R.; Vergniolle, S. 2015. Hawaiian and Strombolian eruptions. *In* The encyclopedia of volcanoes

(Sigurdsson, H.; Houghton, B.; McNutt, S.; Rymer, H.; Stix, J.; editors). Elsevier: 1456 p.

Troncoso, L.; Le Pennec, J-L.; Jaya, D.; Vallee A.; Mothes, P.; Arrais, S. 2006. Depósitos de caída de ceniza producidos durante las erupciones del volcán Tungurahua, 14 de julio y 16 de agosto de 2006. *In* Jornadas en Ciencias de la Tierra, No. 6. Escuela Politécnica Nacional, Departamento de Geología: 181-184. Quito.

Troncoso, L.; Bustillos, J.; Romero, J.E.; Guevara, A.; Carrillo, J.; Montalvo, E.; Izquierdo, T. 2017. Hydrovolcanic ash emission between August 14 and 24, 2015 at Cotopaxi volcano (Ecuador): Characterization and eruption mechanisms. Journal of Volcanology and Geothermal Research 341: 228-241.

Tsunematsu, K.; Bonadonna, C. 2015. Grain-size features of two large eruptions from Cotopaxi volcano (Ecuador) and implications for the calculation of the total grain-size distribution. Bulletin of Volcanology 77:64.

Walker, G.P.L. 1971. Grain-size characteristics of pyroclastic deposits. The Journal of Geology 79: 619-714.

Wohletz, K.H. 1986. Explosive magma-water interactions: Thermodynamics, explosion mechanisms, and field studies. Bulletin of Volcanology 48 (5): 245-264.

Wright, H.; Cashman, K.; Mothes, P.; Hall, M.; Ruiz, A.; Le Pennec, J.-L. 2012. Estimating rates of decompression from textures of erupted ash particles produced by 1999-2006 eruptions of Tungurahua volcano, Ecuador. Geology 40: 619-622.

Manuscript received: February 5, 2017; revised/accepted: October 17, 2017; available online: October 17, 2017.